An Evolutionary Strategies Method to Optimize Turbine and Compressor Blades

by

Noel Cervantes

A thesis submitted to the Graduate Faculty of
Auburn University
in partial fulfillment of the
requirements for the Degree of
Master of Science

Auburn, Alabama
May 5, 2018

Keywords: Compressor, Turbine, Optimization, Shape Functions

Approved by

Roy Hartfield, Walt and Virginia Woltosz Professor of Aerospace Engineering
D. Stephen Nichols, Assistant Professor of Aerospace Engineering
Vrishank Raghav, Assistant Professor of Aerospace Engineering

Abstract

The main goal of this study is to improve a two-dimensional optimization scheme for turbine and compressor blades, specifically by improving the overall efficiency of each blade row with respect to objective and penalty functions. The study will utilize the NASA Energy Efficient Engine high pressure turbine stage 1 and NASA Compressor Rotor 37. Optimization of compressor and turbine blades utilizing a range of advanced learning techniques such as Genetic Algorithms, Evolutionary Strategies, and Neural Networks, have been the subject of numerous studies. This research uses Evolutionary Strategies since it has applicable characteristics which promote speed, reliability, and simplicity of implementation as compared to Genetic Algorithms or Neural Networks. To drive the analysis to an optimal solution, objective and penalty functions will be utilized and discussed as they are used to evaluate each offspring and ensure the optimum solution has the desired flow characteristics. While optimization is critically important for improving the efficiency of the compressor and turbine; of equal or greater importance is the modeling approach used for predicting performance. One element of modeling discussed in this work is the previous use of Bezier Curves and its inability to generate the entire blade, specifically at the leading and trailing edge. An improved method for modeling the blades utilizing “Class” and “Shape” Functions will be implemented as they are useful for controlling the curvature of the leading and trailing edges and still provide the same continuity as Bezier Curves.

Acknowledgements

I would like to thank Dr. Hartfield for advising me on this research project and for allowing me to contact him anytime with questions, without it I would not have been able to complete this thesis. I would also like to thank my mother and my two brothers who continually provided support to me so that I may pursue an advanced degree. Last, I would like to thank the Auburn NSF-AGEP for the technology fellowship, allowing me to purchase a computer to complete this project.

Table of Contents

List of Figures

List of Tables

List of Abbreviations

CST	Class/Shape Transformation
EEE	Energy Efficient Engine
ES	Evolutionary Strategies
HPC	High Pressure Compressor
HPT	High Pressure Turbine
LE	Leading Edge
LPC	Low Pressure Compressor
LPT	Low Pressure Turbine
NURBS	Non-Uniform Rational B-Splines
OBJ	Objective Function
PEN	Penalty Function
TE	Trailing Edge

List of Symbols

A_i	Bernstein Coefficients
B_i^n	Bernstein Polynomials
b_0	Bezier Control Points
C	Class Function
C_p	Coefficient of Pressure
h	Heat Transfer Coefficient
m	Meridional Direction
$\dot{m}$	Mass Flow Rate
N1	Leading Edge Shaping Parameter
N2	Trailing Edge Shaping Parameter
n	Degree of Points
P	Pressure
$P_{net,shaft}$	Shaft Power
R_{LE}	Leading Edge Radius
rθ	Blade-to-Blade Direction
S	Shape Function
St	Stanton Number
T	Temperature
V	Absolute Velocity
W	Relative Velocity
$\bar{w}$	Pressure Loss Coefficient
x	Axial Coordinate
$\bar{x}$	Non-Dimensionalized x-coordinate
z	Streamwise Coordinate
$\bar{z}$	Non-Dimensionalized z-coordinate
Δz	Trailing Edge Thickness
α	Pitch
β	Boat Tail Angle
γ	Specific Heat Ratio
η	Efficiency
λ	Offspring
$\bar{\lambda}$	Diffusion Parameter
μ	Parent
ρ	Density
σ	Mutation Operator
τ	Pressure Ratio
Subscripts	
a	Ambient

ad	Adiabatic
IN	Inlet
EX	Exit
R	Rotor
S	Stator
t-t	Total-to-Total
θ	Tangential Direction
0	Total Conditions

Chapter 1

Introduction

"The next big step for aircraft engine development will be the direct integral optimization of the engine and aircraft as an integrated system." -a paraphrase of comments made by Jan Schilling, former chief engineer for GE as he accepted the AIAA Air Breathing Propulsion Award at the Joint Propulsion Conference, Orlando, FL, July 2015. This statement is a powerful realization that aircraft, especially commercial, have few design changes capable of drastically changing the aircraft such as the propulsion components and aerodynamic shape of the body. Today most commercial airplanes have common components with similar performance characteristics. So, what can be done to improve the performance of airplanes? Jan Schilling's use of a specific word "optimization" to combine the engine and aircraft system as one, affirms that typically when a plane body is made one company designs the body and then an engine is fitted to that plane. However, when an engine is made, it is made to fit a set of design parameters such as thrust available. So, even though both the body and engine are "efficient" in their own respects they have not been optimized together. This idea of optimizing components together to obtain the highest performance is the motivation for this research project. But, before we obtain an optimization between the engine and airplane body, the optimization of the engine components should be shown to be viable. Typically, engine design parameters are initialized and changed slightly to meet requirements. Sometimes those requirements are met, but many design changes

are implemented to meet a more realistic goal. However, recent studies have shown that the use of optimization techniques can allow the maximum performance to be realized. Specifically, for this project, the optimization of the compressor and turbine blades are of interest.

1.1 Motivation

If the performance of the compressor and turbine sections can be improved, it is likely that the overall engine performance can improved. As of today, many engines are reported to have high efficiencies for both the compressor and turbine as shown in Table 1, but there are still improvements that can be made. The goal of this research is to be able to control the aerodynamic flow in the compressor and turbine sections so that the optimum performance may be obtained. A huge motivation for wanting to increase performance of the compressor and turbine section is due to fuel prices required to power jet engines for both power generation and jet propulsion. Shown in Figure 1 below shows the gas price trends for jet fuel and aviation gasoline and one can easily see that trends in price are typically increasing compared to decreasing sections [1].

Table 1. Efficiencies for Past Jet Engines

	EEE	GE90	F100
η_LPC	0.906	--	0.83
η_LPT	0.925	--	0.86
η_HPC	0.861	0.91	0.84
η_HPT	0.927	0.93	0.86

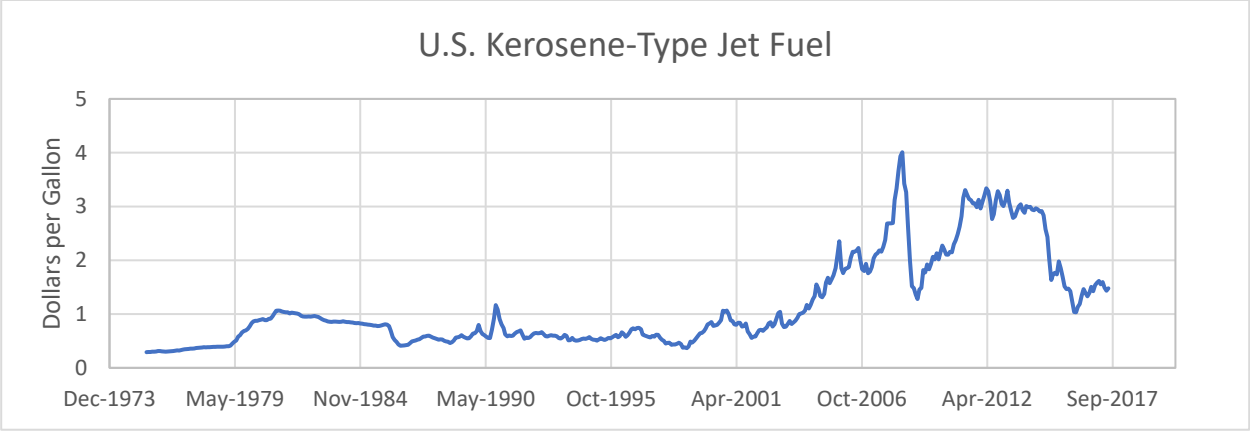

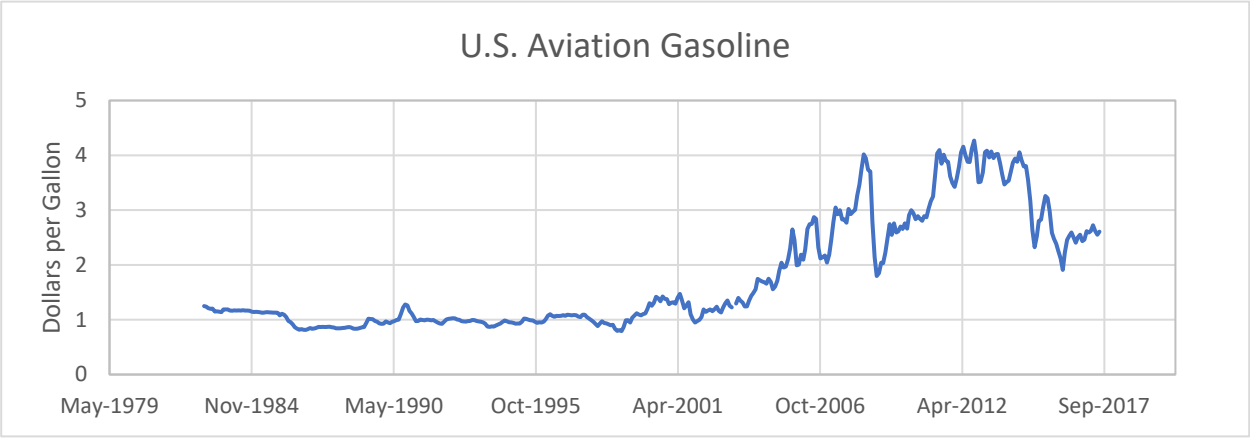

Figure 1. Pricing Trends for U.S. Jet Fuel & Aviation Gasoline

1.2 Goals

Many previous studies have been done to optimize the geometric design of the turbine and compressor blades to improve the components overall performance either by direct, inverse, or a combination of the former. This work itself is a revision of previous studies done by Curriston [2] and Thorn [3]. The importance of this revision will be explained in much detail in the following chapters. There were several goals of this research and the first being able to produce a scheme

which can model stators and rotors for both compressors and turbines, which proved to be the biggest challenge. Second, generating the initial grids from the initial blades to be used for computational fluid dynamic (CFD) studies. The third goal was to be able to use the optimizer previously used from Curriston [2] to optimize the turbine and compressor blades, so that the flow inside the turbine and compressor can be controlled to produce higher performance characteristics.

1.2.1 Goal 1: Blade Modeling

Curriston [2] and Thorn [3], both utilized Bezier curves to effectively model turbine blades for a T55-GA-714A turboshaft engine and a turbine based combined cycle engine for an SR-72, respectively. However, when modeling with Bezier curves, the leading and/or trailing edges must be predefined or fixed to ensure that a continuous curvature is produced so that blades produced are feasible and do not exhibit decreased performance characteristics. To combat this issue, a parametric geometric representation consisting of “Shape” and “Class” functions will be utilized to model the compressor and turbine blades. For the compressor, NASA Rotor 37 is optimized and for the turbine, the NASA Energy Efficient Engine (EEE) high pressure turbine stage 1 is optimized.

1.2.2 Goal 2: CFD Analysis

To analyze the blades, two different computational fluid dynamics tools will be used to automatically generate grids and analyze them. The grid generation tool is called Grids About Airfoils using Poisson’s Equation (GRAPE) [4] and the grid analyzer is Rotor Viscous Code

Quasi-3-D (RVCQ3D) [7] both from NASA Glenn, which allows a user to generate C or O type grids for turbomachinery configurations.

1.2.3 Goal 3: Optimizer Runs

Once the blades are evaluated from the CFD tools, objective and penalty functions are used to rank the airfoil blades for the optimizer scheme. To optimize the blades, an optimizer called Evolutionary Strategies (ES) is used. ES is an adaptive optimizer, which uses a mutation algorithm to generate new offspring (λ) based on the current parent (μ) to drive the solution to an optimal one.

1.3 Literature Review

As of today, there is a large amount of research on turbine and compressor design, but not a significant portion which utilize adaptive optimizers. Optimization itself is a niche area of research; however, it has many applications, which make it widely popular, ranging from store layout to missile design. Fortunately, there are many research papers and books, which detail design methods and CFD methods for turbomachinery. Since this study is not a purely CFD research project the CFD schemes were not compared to other available schemes outside of GRAPE and RVCQ3D. The CFD solver validation was based mostly on the work from Curriston [2][8][9], Thorn [3][10][11], and Chima [12][13][14][15][16].

For the turbine and compressor analysis, several textbooks which outline turbomachinery design and turbine/compressor aerodynamics were used to understand the fundamentals of turbomachinery rotor and stator design and understand how the aerodynamic flow is affected by

geometric changes. The most useful texts were those of Baskharone [17], Flack [18], Cumpsty [19], Wilson & Korakianitis [20], Aungier [21][22], and Hill & Peterson [23]. Baskharone, Flack, and Hill & Peterson are by far the most useful for understanding the basics of turbomachinery flow such as the velocity diagrams for both the rotors and stators and learning the vast amounts of terminology related to turbomachinery. The author would recommend those as advanced undergraduate texts to get started in turbomachinery. Cumpsty, Wilson & Korakianitis, and Aungier are more advanced texts and are recommended for graduate students as they assume you understand the basics of turbomachinery flow. However, they were the most helpful for this research project in that they go more into design philosophy of compressors and turbines and the texts show many in depth studies that show just how important the geometry can alter the flow.

Although, optimization has been around for many decades, this approach to design is just now permeating mainstream conceptual and preliminary design activities in aerospace sciences. There are a few exceptions, one being neural networks and its ability to analyze and predict large sets of data for compressors, which is a current major focus of research. However, this project focuses on using only the Evolutionary Strategies optimization scheme. Again since this project is a revision, comparison studies will not be presented since it was previously shown in Curriston [2] and Thorn [3] that Evolutionary Strategies was the most useful optimizer for single blade row optimization. But to inform readers of the most useful resources pertaining to Evolutionary Strategies, a few will be mentioned. The most useful literature available that the author currently uses is *Metaheuristics for Hard Optimization Methods and Case Studies* by Dreo [24]. This text shows the user the fundamentals of Evolutionary Strategies and even provides a skeleton code so that the user may start to code an algorithm of their own. Also, many prewritten codes and software versions are available on the internet, which provide very useful examples. However, since

Evolutionary Strategies is not a complex problem to understand, it is recommended that the user simply write his or her own code.

For the blade modeling algorithm, the author was initially using Bezier Curves to model the turbine and compressor blades. However, due to issues of flexibility and fidelity described in Chapter 2, the author decided to use a Parametric Geometry Representation consisting of "Class Functions" and "Shape Functions" to have more control of the geometry of the blades. This method of representation shows that one can easily control the leading and trailing radius and implement a full three-dimensional analysis without having to utilize hybrid schemes such as the Non-Uniform Rational B-Splines (NURBS) [25]. Kulfan & Bussoletti [26], who was the most useful work, show the derivation of the "Class Functions" and "Shape Functions". Kulfan & Bussoletti show many different geometries which can be made ranging from pointed wedges to blunt faced objects. This parametric geometry representation will be the basis for modeling and will contain the mutation points needed for the optimization scheme.

1.4 Preliminary Design Parameters

When designing many engineering technologies, typically design goals are defined. Similarly, with turbomachinery the compressor and turbine section both have defined goals and to meet these goals design parameters are calculated. This method is called direct blade design [20] and usually consists of engineers starting off with the two-dimensional velocity triangles to calculate inlet and exit conditions for total pressure, Mach number, flow angles, etc., then experiments are conducted to generate blades which match the design parameters. Blades are also

pulled from databases that have already been researched to decrease the design process iteration. The main issue with direct blade design is that it is a tedious time-consuming process.

To decrease the amount of time designing blades, an inverse design method [20] is implemented which guesses an initial airfoil and using computational solvers the blades are analyzed to see if they match the design parameters. Just as direct design, inverse design has issues with the computational solvers being used because experiments do not always match with computational results. Computational costs also effect the design phase increasing resources required.

To get the best of both worlds, this project will assume that some direct design has been accomplished to obtain an efficient blade design. So, this project will rely more on inverse design to obtain a blade which matches design criteria. Utilizing initial data sets are therefore required, which is why NASA Rotor 37 and the EEE HPT stage 1 were chosen. They both have vast amounts of publicly available data and the initial CFD data was able to be reproduced using GRAPE and RVCQ3D. The initialized data consists of the inlet boundary conditions, number of blades, blade speed, meridional location, and the stream surface radius and thickness.

Chapter 2

Blade Modeling

Initially the author was to optimize the compressor and turbine blades using Bezier curves so that a three-dimensional model of the compressor and turbine could be performed. At first, modeling the turbine was quite simple as it was already shown in detail from Curriston [2] and Thorn [3] that Bezier curves were a good modeling tool. However, when it came time to model NASA Rotor 37, issues not seen previously with the turbine section arose and could not be handled. As time passed, the author received information from their professor about “Class” and “Shape” functions being used to model propeller blades done by a previous Auburn University Graduate student, Christoph Burger [27]. This chapter will detail issues with using Bezier curves and work-around solutions that are typically used in previous studies to model blades.

2.1 Initial Bezier Curve Analysis

To begin the author initially started with Bezier curves and achieved good success modeling the turbine blades. Modeling the blades does require control points that the Bezier curves use to generate coordinate points for both the x and y directions. Acquiring these coordinates are quite simple, and the author used Evolutionary Strategies with a least squares minimization

objective function to minimize the error between the exact coordinates and the calculated coordinates from the Bezier curves, as shown in Eq. (2.1).

$$Obj = \min\left(\sqrt{(X_{Actual}^2 - X_{Bezier}^2)} + \sqrt{(Y_{Actual}^2 - Y_{Bezier}^2)}\right) \tag{2.1}$$

2.1.1 Bezier Curve Mathematics

Before the issues with Bezier curves, the mathematics of how Bezier curves work will be shown. There are many derivations in texts outlining how to use Bezier curves, the text used by the author is *The Essentials of CAGD* by Farin & Hansford [25], which shows how to model Bezier curves of any degree. Named after Pierre Bezier, Bezier curves, which are often called "French Curves", are curves mathematically defined by polynomials and are commonly used for computer aided design software packages because they can quickly generate smooth continuous surfaces. Shown in Eq. (2.2) is the Bezier curve of degree n. The b_0 are the Bezier control points and the $B_i^n(t)$ terms are the Bernstein Polynomials, which are shown in Eq. (2.3).

$$X(t) = \begin{bmatrix} x(t) \\ y(t) \end{bmatrix} = b_0 B_0^n(t) + b_1 B_1^n(t) + \cdots + b_n B_n^n(t) \tag{2.2}$$

$$B_i^n(t) = \binom{n}{i}(1-t)^{n-i}\, t^i \tag{2.3}$$

$$\binom{n}{i} = \begin{cases} \dfrac{n!}{i!(n-i)!} & \text{if } 0 \le i \le n \\ 0 & \text{else} \end{cases} \tag{2.4}$$

From Eq. (2.3) & (2.4), one can notice that the accuracy is dependent on degree n and dependent on the binomial coefficients, which are just the coefficients from the (n+1) row on Pascal's Triangle, shown in Figure 2. As an example, for degree n = 4 the Bezier curve equation

is shown below in Eq. (2.5). The initial EEE stator 1 blade is shown in Figure 3 using a degree of 5, which are 6 control points required to be calculated from the least squares minimization and in Table 2 are those calculated control points. As one can see, for the blades the Bezier control points are required for the x and y coordinates.

1

1 1

1 2 1

1 3 3 1

1 4 6 4 1

1 5 10 10 5 1

1 6 15 20 15 6 1

1 7 21 35 35 21 7 1

1 8 28 56 70 56 28 8 1

1 9 36 84 126 126 84 36 9 1

1 10 45 120 210 252 210 120 45 10 1

Figure 2. Pascal's Triangle

$$X_0^4(t) = b_0(1-t)^4 + 4b_1(1-t)^3 t + 6b_2(1-t)^2 t^2 + 4b_3(1-t)t^3 + b_4 t^4 \qquad (2.5)$$

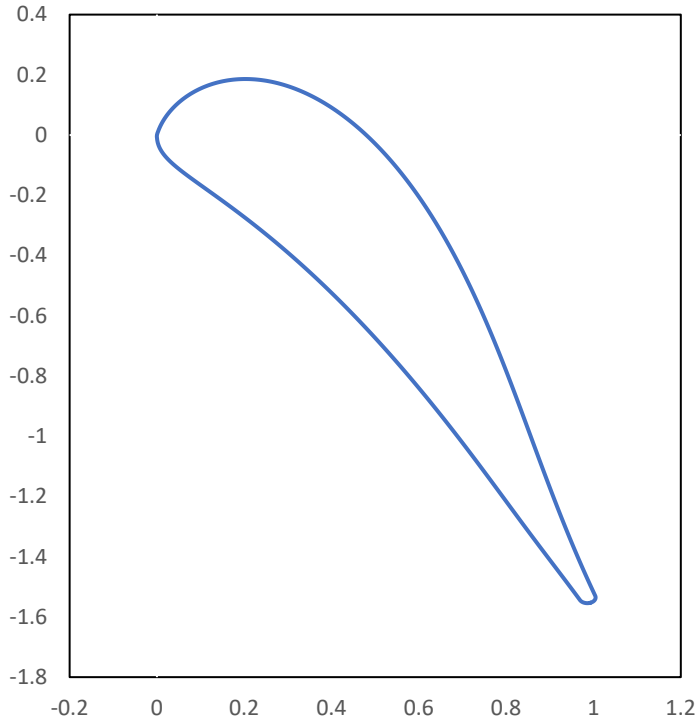

Figure 3. Initial EEE Stator using Bezier Curves

Table 2. Bezier Control Point for Initial EEE Stator 1

Control Point	Suction		Pressure	
	X	Y	X	y
1	0	0	0	0
2	0.04718	0.24349	-0.00401	-0.21520
3	0.44430	0.50342	0.38458	-0.14420
4	0.76357	-0.33887	0.78315	-1.24670
5	0.77490	-0.82601	0.78745	-1.18663
6	1.00385	-1.52955	0.96884	-1.54402

2.1.2 Bezier Curve Problems

Typical iteration counts were around 3000-5000 generations taking about 3 minutes. However, the trailing edge was defined by a circular radius to ensure that the trailing edge was continuous, which was acceptable for the turbine case. But, when applying the Bezier curve to model the compressor blades, the Bezier curves cannot handle small curves with large sets of coordinates, which is required for an accurate computational fluid dynamics analysis. This is because Bezier curves tend to become discontinuous and highly nonlinear for small sharp turns and turbine blades are bulkier and thicker compared to compressor blades, which are thin and sharp. Mathematically speaking, as mentioned earlier the Bezier curves are heavily influenced by the binomial coefficients in Eq. (2.2), which is the reason why the Bezier curves cannot form the leading and trailing edge accurately.

There are some advanced techniques for trying to deal with issues similar. From [25], one can simply increase amount of control points, which sometimes is necessary; however, this introduces problems related to optimization, particularly the mutation because if more control points need to be mutated then more control points need to be optimized, thus greatly increasing the amount of time, which is not feasible for this project, so increasing the amount of control points is not a reasonable solution. Another issue caused by increasing the amount of control points also decreases the stability of the Bezier curve. Farin & Hansford [25], effectively display this issue by showing a semicircle that has an x coordinate slightly modified, resulting in a noncircular shape at the edges and this is called an ill conditioned process, as shown in Figure 4. The top curve shows

the original semicircle and the bottom curve shows the grey x-coordinate that has been modified causing a significant error.

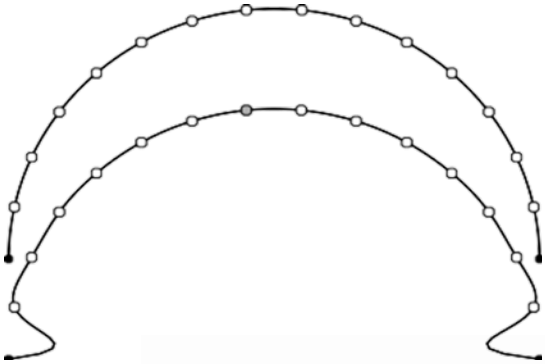

Figure 4. Ill-Conditioned Results using Bezier Curves

2.1.3 Previous Research Studies & Bezier Curves

The next attempt would be to separate the section of the blade and do a piecewise Bezier curve formulation. This could be done by separating the leading edge, trailing edge, and the rest of the blade, so there would be three sections. Typically, the leading and trailing edges are predefined by circular and/or parabolic functions with the center portion made using Bezier curves or other polynomial fits. From Samad & Kim [28], to produce the compressor blades using Bezier curves, they fixed all the control points except for one point in the middle and the leading and trailing edges are not even circular or parabolic. Figure 5 shows this in (a) where the leading and trailing are fixed sharp points and the only point that is modified is P3, which only controls thickness of the blade, and the bottom pressure side is also a fixed spline curve [28]. This shows that the optimization scheme cannot explore the entire search space, thus reducing the optimizers

ability to reach a truly optimal solution. Also, the leading and trailing edges are fixed sharp points in that they do not exhibit physical compressor blades, which are “sharp”, but technically Rotor 37 does have rounded leading and trailing edges. Therefore, their computational analysis is not completely accurate because blades which are truly sharp exhibit less performance loss characteristics.

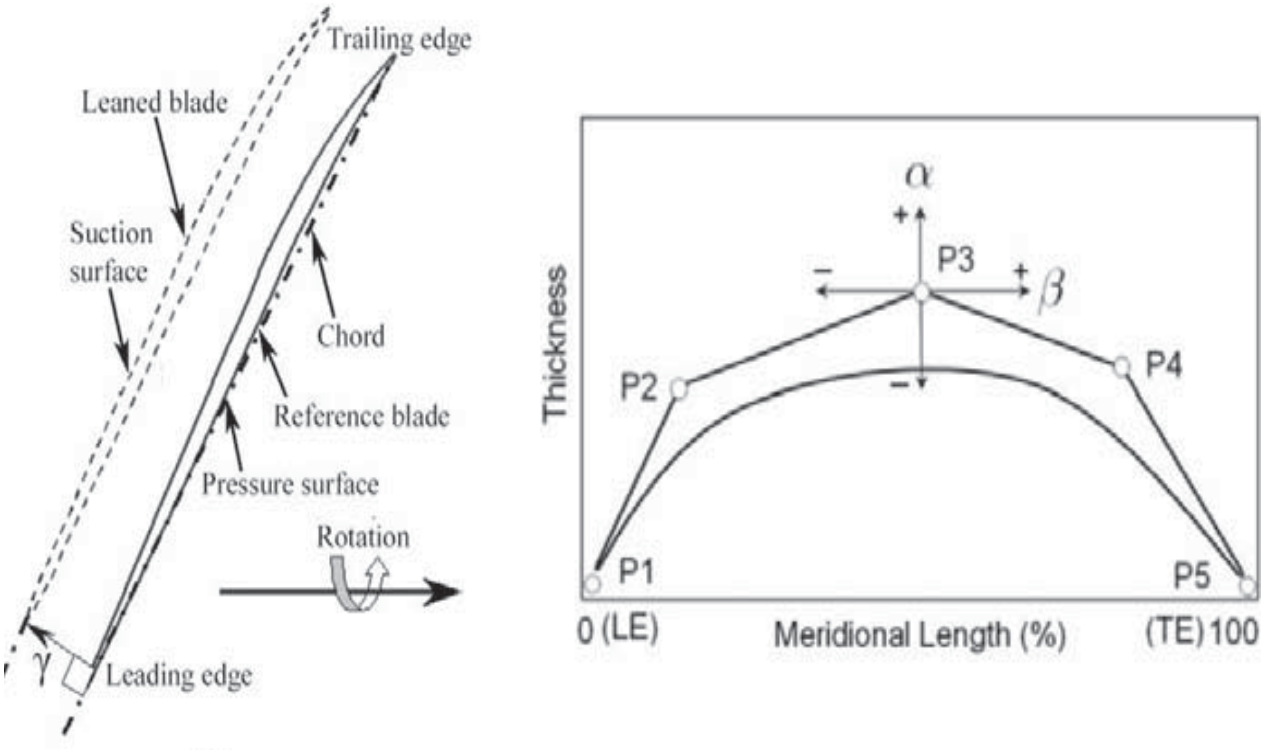

Figure 5. Rotor 37 from Bezier Curves (a); Control Points used for Bezier Curves (b)

2.1.4 Research Setback with Bezier Curves

Many months were spent trying to force the Bezier curves to achieve a good representation of Rotor 37. A few blades did come close, however either the leading or trailing edge would not

converge to the actual coordinates within a few percent. Figure 6 shows the issues with trying to obtain the initial control points for Bezier curves. Clearly, the blade did not converge to actual coordinates during the midspan and at the leading and trailing edges. From Figure 7, two very common issues with Bezier curves are displayed. On the top suction side displayed in pink, the coordinates cross each other, which for blades is a non-physical solution. For the bottom pressure side in blue, the coordinates are displayed in a very nonlinear way because the radius of the leading edge is very small and constitutes a small percentage of the blade chord length. In Figure 8, the

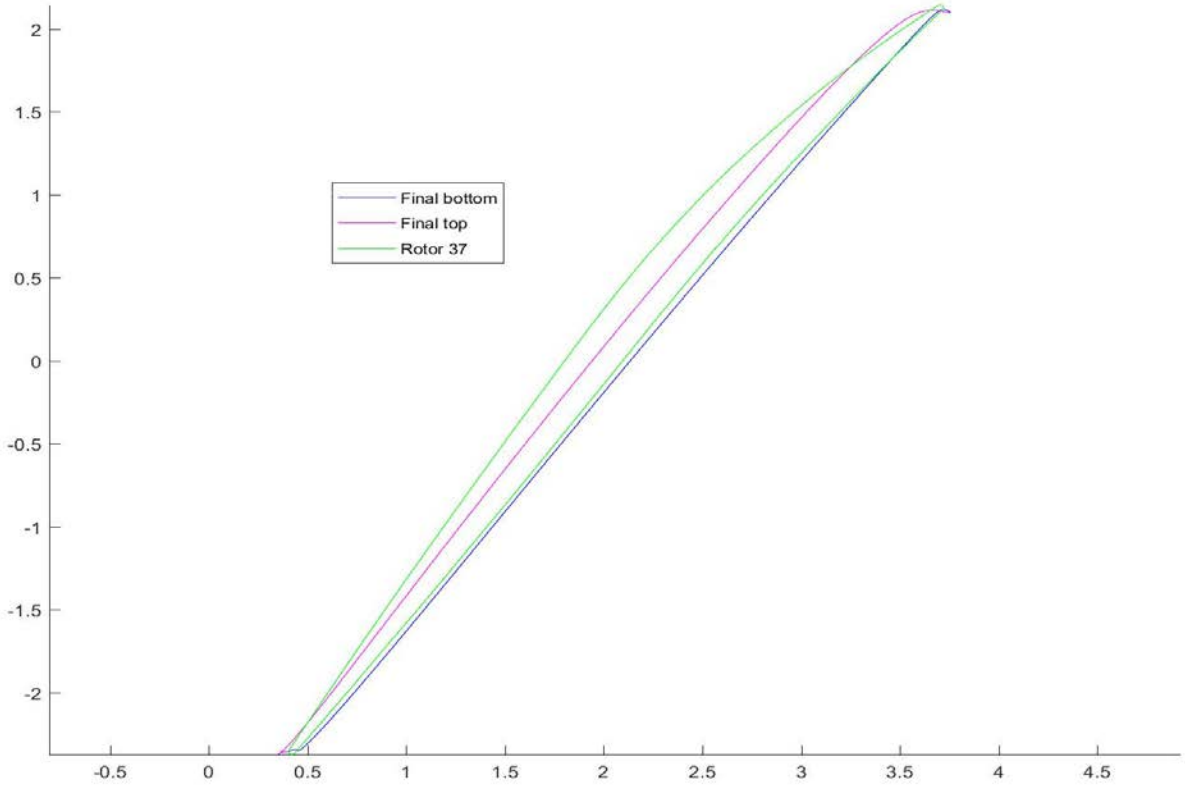

Figure 6. Least Squares Minimization Result for NASA Rotor 37

top suction side and the bottom pressure side are crossing, and the Bezier curve does not even generate a rounded edge. Again, this is a non-physical blade and these non-physical blades are bad for the optimization scheme because once passed to GRAPE to generate grids, it will automatically fail because GRAPE has internal code which tries to generate continuous curves by solving

Poisson's Equations. Failures are bad for the optimizer because they contribute to computational time required to reach an optimal solution.

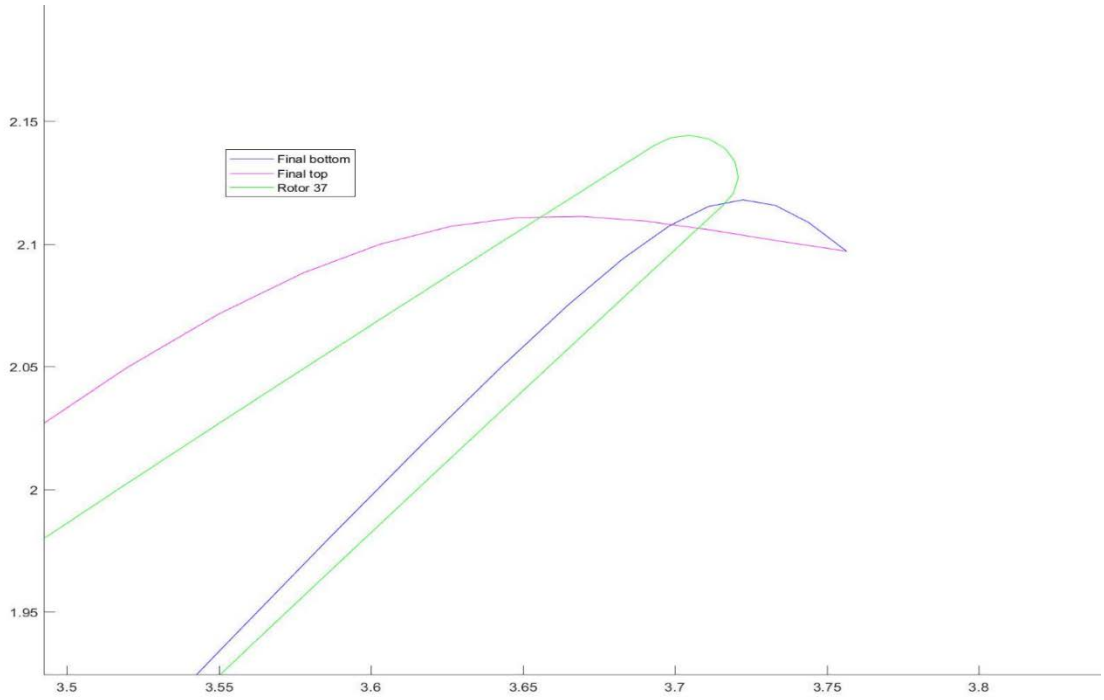

Figure 7. NASA Rotor 37 Trailing Edge from Least Squares Minimization

To simply resolve the issue with most blade models, usually the leading and trailing edges are predefined by some circular and/or parabolic configuration and then points between the blades are interpolated by use of Bezier curves or polynomial expressions. But if the leading edge is predefined, the flow will always be predefined and when performing optimization studies the search space may be reduced causing a nonoptimal solution. So, to be able to generate blades which can produce a leading and trailing edge with feasible and physical curvatures a new method will be implemented for more control.

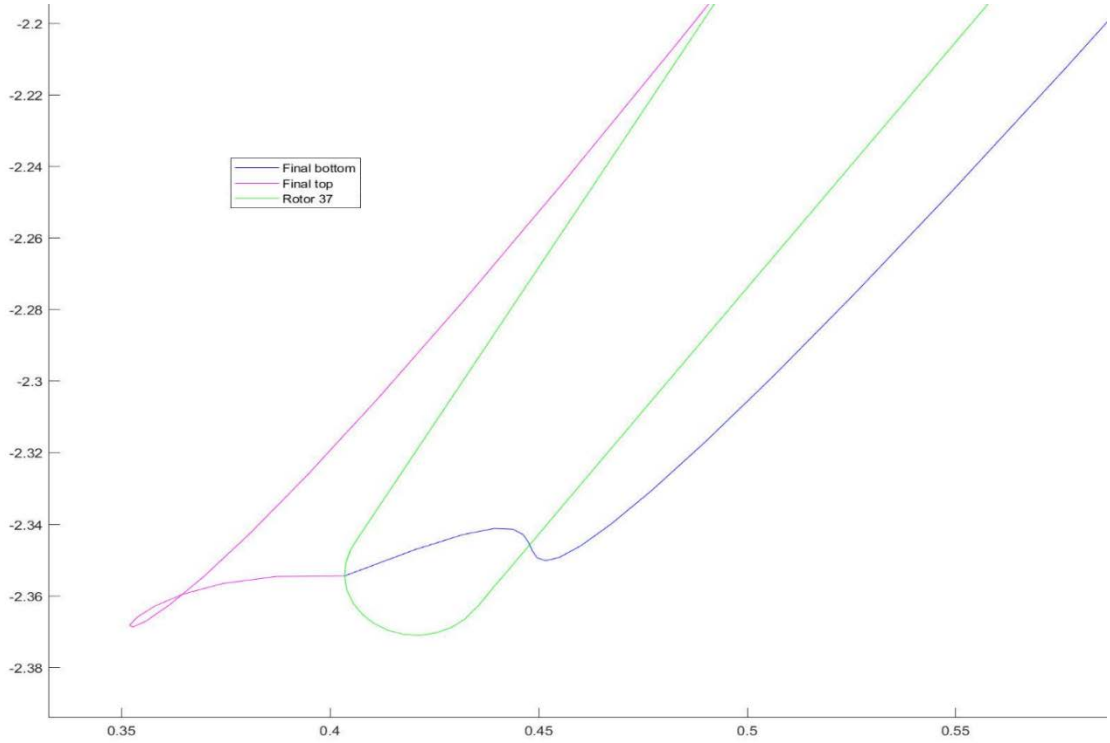

Figure 8. NASA Rotor 37 Leading Edge from Least Squares Minimization

2.2 Parametric Geometry Representation

To improve the methodology for generating blades, a relatively new method has been implemented. Developed in 2006 by Kulfan & Bussoletti [26], their method allows for a unified geometric description of design shapes for airfoil type blades such as aircraft wings, helicopter rotors, and obviously turbomachinery blades and can even do body cross-section types shapes such as fuselages, channels, ducts, and nacelles. Since there is no decided formal name for this parametrized geometry method, the author will further reference the method as the Class/Shape Transformation (CST) surface parameterization Method.

2.2.1 Mathematics of the CST surface parameterization Method

The CST Method is actually very similar to the Bezier curve method in that they both make use of Bernstein Polynomials. Utilizing “Shape” Functions allows the mathematical control of the leading and trailing edge by making use of “Class” functions. The “Class” function is a simple mathematical function consisting of two shaping parameters, which control the leading and trailing edge and is shown in Eq. (2.6). N1 controls the leading edge and N2 controls the trailing edge. Since the “Class” function controls the leading and trailing edges, the “Shape” function term itself generates the entire blade and the “Class” function deforms the leading and trailing edge.

$$C\left(\overline{x}\right) = \overline{x}^{N1}\left(1-\overline{x}\right)^{N2} \tag{2.6}$$

$$\overline{x} = \frac{x}{chord} \tag{2.7}$$

The “Shape” function is the part that is most like the Bezier curve mathematics where they both have Bernstein polynomials, but the “Shape” function has a slight difference.

$$S\left(\overline{x}\right) = \sum_{i=0}^{n} A_i B_i^n\left(\overline{x}\right) \tag{2.8}$$

$$B_i^n\left(\overline{x}\right) = \binom{n}{i}\left(1-\overline{x}\right)^{n-i}\overline{x}^{i} = \frac{n!}{i!\left(n-i\right)!}\left(1-\overline{x}\right)^{n-i}\overline{x}^{i} \tag{2.9}$$

Bezier control points dominate the Bezier curves, whereas in this derivation the “Shape” functions are dependent on Bernstein coefficients (A_i) as seen in Eq. (2.8), which are used to generate the blade coordinates. The way the CST Method generates points is also different than Bezier curves. Bezier curves require two sets of x and y Bezier control points, whereas the Shape Function Method only requires a blade chord length, set of x coordinates ranging from zero to the blade chord length, Bernstein coefficients, and the shaping parameters. The full equation for generating

the blade coordinates are shown in Eq. (2.10), where the $\Delta\bar{z}$ term allows the blade to have a trailing edge thickness.

$$\bar{z} = \frac{z}{chord} = C(\bar{x})S(\bar{x}) + \bar{x}\bullet\Delta\bar{z} \tag{2.10}$$

2.2.2 Effects of the Shaping Parameters

Assuming a "shape" function value of unity, Figure 9 shows the effects of changing the shaping parameters [26]. One can see the wide range of variability that the shaping parameters provide from flat faced bodies to sharp wedges with rounded trailing edges.

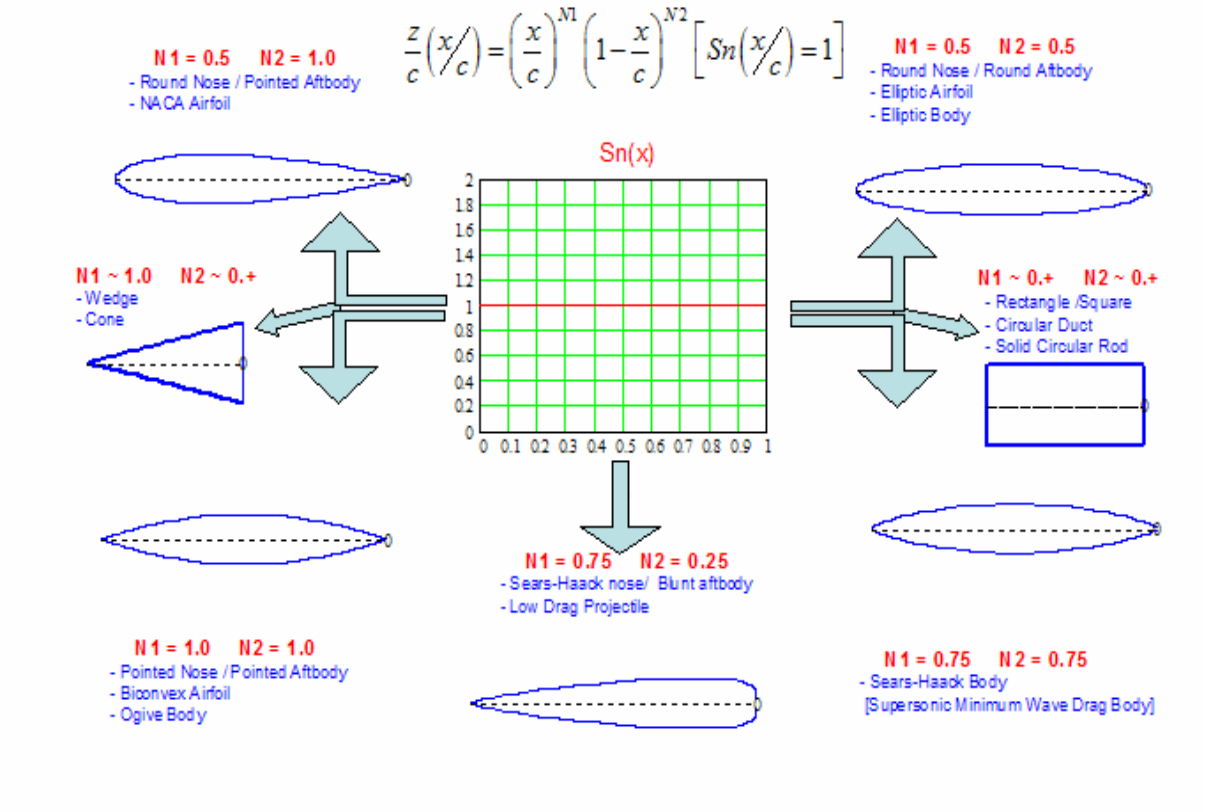

Figure 9. Effects of the Shaping Parameters

Aside from being able to control the leading and trailing edges, the CST Method has several other useful qualities as well. First, the parameters within the Bernstein polynomials do not have any effect on the leading and trailing edges anymore because of the combinational effect from the

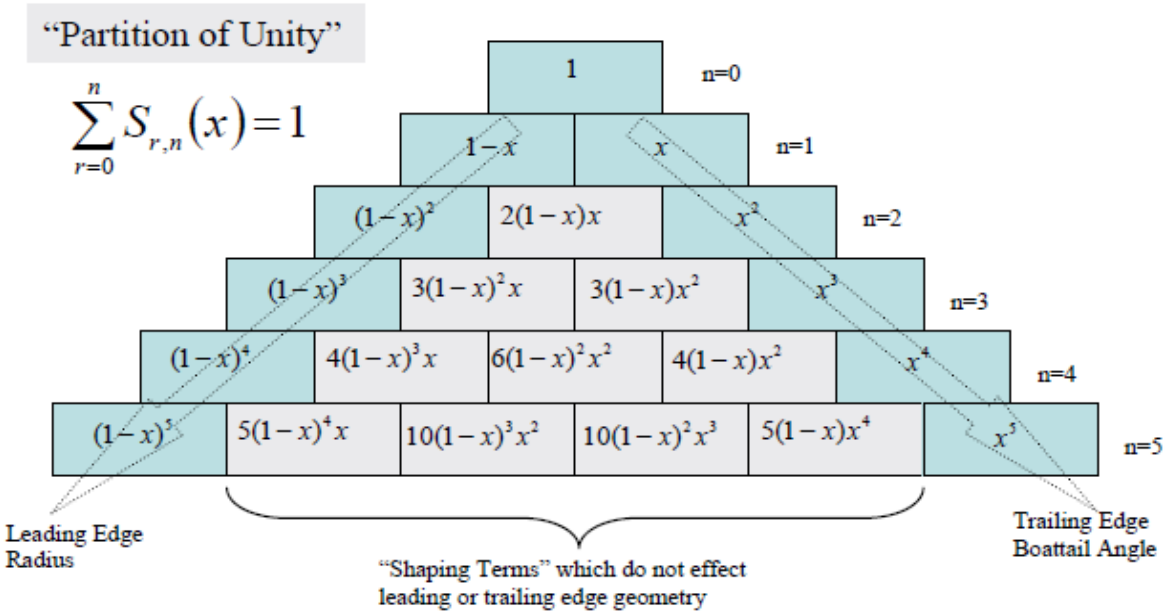

Figure 10. Effects of "Shaping Terms" on the LE & TE

Bernstein Coefficients and the shaping parameters, which is shown in the Pascal's Triangle in Figure 10 [26]. So, the problem shown in Figure 4, which was a big issue with generating the compressor blades, is not involved with the CST method and no longer an issue in this project. Also from [26] a derivation, which directly equates the Shape Function values at the leading and trailing edge location and shown in Eq. (2.11) and (2.12), respectively.

$$S(0) = \sqrt{\frac{2R_{LE}}{chord}} \tag{2.11}$$

$$S(1) = \tan\beta + \frac{\Delta Z_{TE}}{chord} \tag{2.12}$$

2.2.3 Initial Blades Generated from the CST Method

Now, that the mathematics have been defined, applying them to generate the initial blades can now proceed. The Least Squares Minimization is used with the Evolutionary Strategies algorithm to generate the z coordinates, Bernstein Coefficients, Leading/Trailing edge shaping terms, and the ΔZ. Also, the pressure side is separated from the suction side because the one drawback of the CST method is that an equation cannot be made for a complete revolution. The Bezier cannot easily do that either, at least not for turbomachinery blades. So, two sets of data must be optimized to obtain both the suction and pressure side coordinates, which are relatively easy to converge. The time for convergence was 5 minutes for all three blade cases.

The first blade that was generated was the NASA EEE HPT Stator 1, shown on Figure 11. The next blade is NASA EEE HPT Rotor 1, shown on Figure 12.And the reason for using the CST method, NASA Rotor 37 in Figure 13.

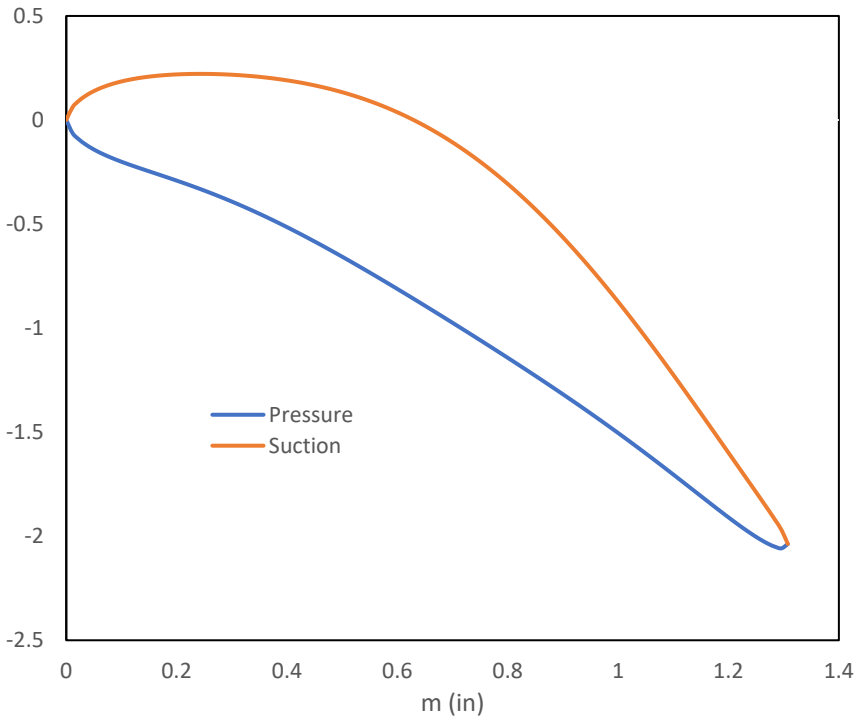

Figure 11. Initial EEE Stator 1 from CST

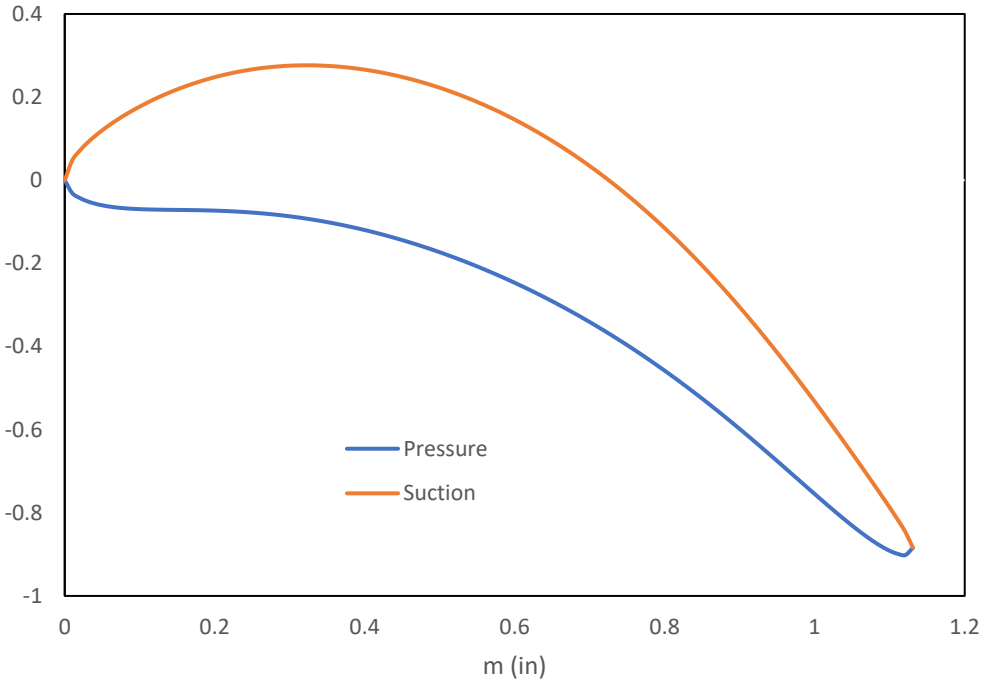

Figure 12. Initial EEE Rotor 1 from CST

Table 3, shows the parameters required to generate the initial blades, excluding the coordinates. There are 15 CST parameters, which is a large search space, so there are many variables that can optimized for. However, due to the many parameters there could be an infinite amount of combinations which contribute to the optimizer. To ensure the optimizer does not take forever, the author decided that only the Bernstein coefficients needed to be altered, so only ten parameters need to be mutated. The leading and trailing edge parameters do not need to be altered because the curvature will be altered by A1 and A5. Also, ΔZ and the chord length were not mutated because the author did not want to alter the solidity of the blade, which is the ratio of the blade chord length to the blade pitch, therefore reducing the performance and possibly the structural integrity.

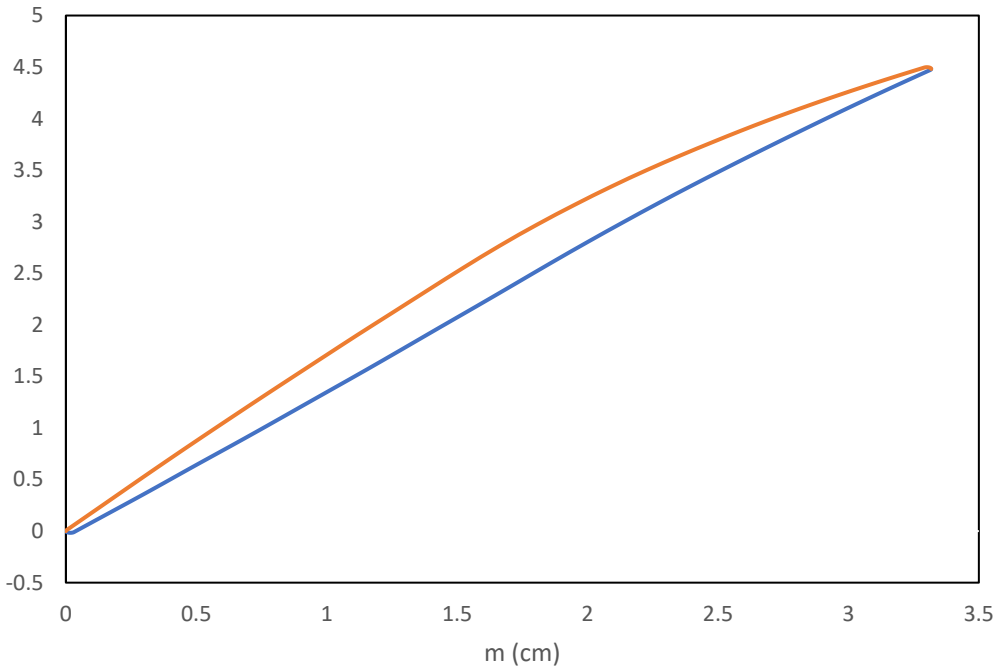

Figure 13. Initial Rotor 37 from CST

Table 3. CST Parameters for Each Blade

	EEE Stator 1		EEE Rotor 1		Rotor 37	
	Suction	Pressure	Suction	Pressure	Suction	Pressure
A1 (LE)	2.21915	0.53908	1.03484	0.23403	0.29901	0.27777
A2	1.87453	-0.96509	1.71931	-0.65508	1.19050	-0.32529
A3	3.11201	0.32906	1.37236	-0.30173	1.29573	0.32126
A4	2.40011	-0.73771	1.99818	-0.74762	1.36937	-0.63459
A5 (TE)	0.80021	0.45443	1.99818	0.29343	0.49909	0.041455
ΔZ	-2.664		-1.0000		14.8669	
N1	0.7000	0.6000	0.6220	0.4582	0.6224	0.3843
N2	0.5000	0.5000	0.7152	0.4912	0.5373	0.3275
chord	1.3075		1.1309		3.3173	

Chapter 3

Optimizer Schemes

Many adaptive optimizers that have been applied with much great success. This project deals solely with Evolutionary Strategies. Although, many other optimizers have been applied to turbomachinery optimization, especially Genetic Algorithms. Choosing an optimizer which is appropriate for turbomachinery is quite straight forward. Either choose an optimizer for continuous problems or combinatorial problems. A combinatorial problem has an exact finite number of possibilities. A famous example is the Quadratic Assignment Problem and is commonly used for location problems, such as assigning r amount of facilities to r amount of locations. Optimizers best suited to tackle this problem would be Tabu Search or Ant Colony. Since these types of problems do not apply to turbomachinery, an optimizer more suited to solve continuous problems are required. A continuous problem is a problem that has infinite solutions, just as turbomachinery does. There are an infinite number of blades that can have a set performance, but only a set of which have the max performance for a given set of design parameters. Therefore, an optimizer which can solve problems with an infinite search space are required. Most suited optimizers are Evolutionary Strategies, Genetic Algorithms, Particle Swarm Optimizers, and Differential Evolutions. These optimizers will be briefly described to compare their differences and will not be applied in this project, as for reasons that will be mentioned.

3.1 Genetic Algorithms

Based on biology Genetic Algorithms, mimic real-world evolution by mutating genes in a bit string to have improved characteristics such as Darwin's Finches. Just as real-world evolution works, Genetic Algorithms are slow to mutate and generate an optimal solution, which is partly why they were not chosen for this project and more specifics can be found from *Metaheuristics for Hard Optimization* [24]. Like Evolutionary Strategies, the only difference between the two is the mutation and replacement of generated solutions. Genetic Algorithms work in the following order: Initialization of parameters; Calculate initial fitness; Select two parents (λ) considering their fitness and generate two children or offspring (μ) based on probability; Mutate the children based on mutation probability, which is very small; Evaluate children and replace the parents if the children are better (minimization or maximum), repeat until the max number of generations condition is met. So, really the only difference between Genetic Algorithms and Evolutionary Strategies is that mutation does not always occur for the children. Because of this quality, Genetic Algorithms take a significant amount of time compared to Evolutionary Strategies and requires a larger search space to explore solutions compared to Evolutionary Strategies.

3.2 Particle Swarm Optimizer

Originally based on socio-psychology for data processing and social group decision-making, Particle Swarm Optimizers are relatively new compared to Genetic Algorithms and Evolutionary Strategies and more specifics are found in [24]. Typically, Particle Swarm Optimizers are analogized to birds changing course in flight or a school of fish evading a predator. Particle Swarm Optimization is far different from Genetic Algorithms and Evolutionary Strategies

in that particles in the search space are updated from their initial position based on their velocity. Velocity is then updated based on the particle with the best fitness in the neighborhood of particles, so particles influence each other. There are issues related to Particle Swarm Optimizers, particularly dealing with the velocity. The velocity has the most influence as it controls where the particle moves in the search space so if the velocity blows up then the particle moves very far, but there are many proposed ways of dealing with this. Also, if a new optimum solution has been found after convergence, then particles will start to swarm to the new optimum solution space. This could prove troublesome, because it means that Particle Swarm Optimization is likely to get caught in a local optimum and if it does manage to get out of the local optimum after convergence, it will take the algorithm even more time to converge again. Therefore, due to time constraints again, Particle Swarm Optimization has not been chosen for this project.

3.3 Differential Evolutions

An Evolutionary Algorithm similar to Genetic Algorithms and Evolutionary Strategies, Differential Evolutions is also a population-based optimizer that mutates the offspring to drive the solution to an optimal one. Designed solely for continuous problems, Differential Evolutions is highly capable of solving non-differentiable, nonlinear, and multimodal functions and only requires a few parameters. The main differences from the other Evolutionary Algorithms are as follows: Offspring are created by more than two parents; Mutation is also affected by two or more parents; Parents are compared to the offspring one-on-one rather than combining the entire family and choosing the best ones. Differential Evolutions has several features related to its initial selection for this work. One, if the search space is too similar than the mutation can stagnate and will not improve. It is not as effective with many design parameters that need to be optimized and

is meant more for multimodal optimization. Multimodal optimization looks to find a set of optimal solution which are objectively equivalent, but in different local optima space. This project is only focused on the final optimized solution, based on multi-objective functions, therefore Differential Evolutions is not appropriate for this project.

3.4 Evolutionary Strategies

As the title of this project suggests, Evolutionary Strategies (ES) was the chosen optimization scheme used to calculate an optimal solution. ES was used with great success by Drew Curriston [2], previously at Auburn University. Again, the only difference between ES and Genetic Algorithms is the mutation scheme where in ES, every parent generates an offspring and every offspring is mutated by some mutation operator value. The algorithm for ES is quite simple to understand and implement. ES has been implemented for many types of problems such as global/local minimum and maximum problems. An example, would be to solve the Ackley Function, shown by Eq. (3.1) and plotted on Figure 14. The Ackley Function has a global minimum at f(x,y)=f(0,0)=0 bounded in the space -32<x,y<32. This is a typical problem that is solved to ensure validation of the optimizer because there are many local minimum solutions and only one true global minimum. ES has been verified to solve this function by the author.

$$f(x,y) = -20\exp\left(-0.2\sqrt{0.5\left(x^2+y^2\right)}\right) - \exp\left[0.5\left(\cos\left(2\pi x\right)+\cos\left(2\pi y\right)\right)\right] + 20 + e \qquad (3.1)$$

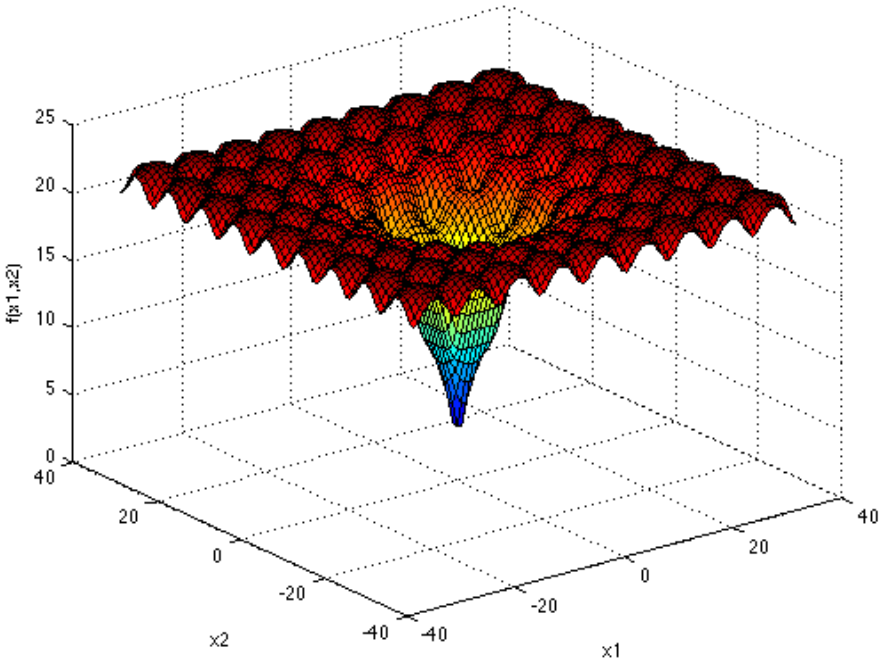

Figure 14. Ackley Function

3.4.1 ES Algorithm Flow

As mentioned earlier, the ES algorithm is simple to understand by Figure 15. Each major component of ES will be outlined in this subsection. Also included in Appendix A, is the skeleton code for the ES Algorithm. First the type of problem is first identified, which has been discussed briefly in the previous sections of this chapter. For this project, optimizing for the blades is a continuous problem because there are many types of blades that can be used. An infinite number of blades can be used, ranging from bad performance to high performance. It is the goal of this project to get the best one. To classify this problem based on difficulty, one would label it NP-Hard because there is an unknown number of parameters which define the optimal solution.

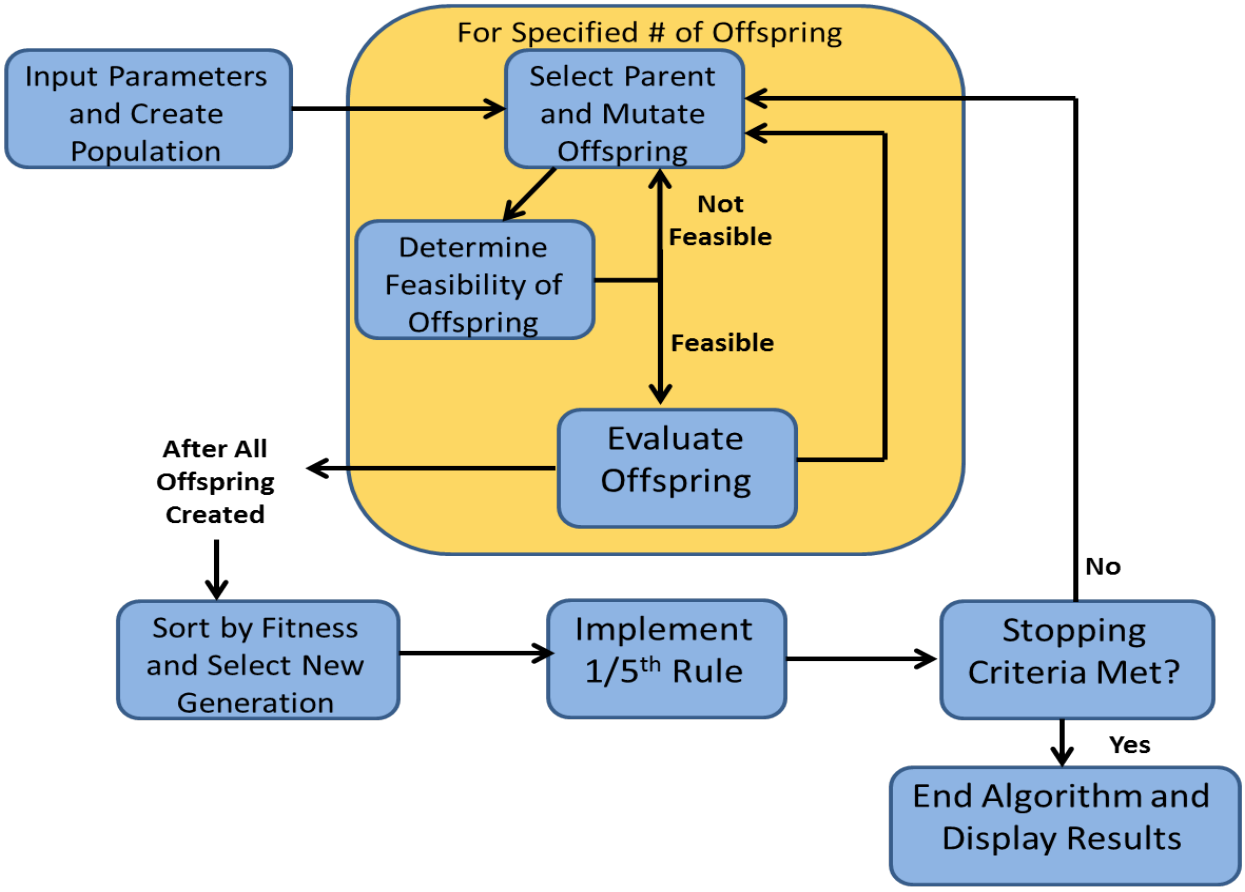

Figure 15. ES Algorithm Flow

Typically, in optimization a random solution is first defined, but it is the goal of this project to optimize already designed blades for validation, which are NASA Rotor 37 and the NASA EEE HPT Stage 1 blades. Second, the initial blade is then evaluated to obtain an initial objective value. Then offspring are produced, and for this project 4 parents are chosen and for each parent 2 offspring are made. Once the offspring are made, they are each evaluated using CFD tools, which are defined in the next chapter along with the objective functions. Next, all the parents and offspring are ranked and only the best four are kept. While this is happening the history of the solutions are stored so that the one-fifth rule may be applied to change the mutation. The one-fifth

rule states that if greater than one-fifth of the solutions are better than the parents the mutation operator (σ) is increased to diversify the search space, which is shown by Eq. (3.2).

$$\sigma = 1/\left(0.85\sigma\right) \tag{3.2}$$

The philosophy behind this approach is that the solutions are starting to explore a more optimal search space, so the mutation is increased such that the search space can be explored more aggressively. If less than one-fifth of the solutions are better than the parents, the mutation operator is decreased to lessen the search space. This means that the solutions are starting to explore a space which yields less optimal solutions, so to make the solutions go back to the optimal space, we decrease the mutation, as shown in Eq. (3.3).

$$\sigma = 0.85\sigma \tag{3.3}$$

For the EEE rotor, σ equals 0.05 and for the EEE stator σ equals 0.1 and rotor 37 σ equals 0.01. So, once the blades are ranked and the mutation operator is updated, the entire process repeats many times until the final condition is met and for this project a set number of max generations is set to 100 compared to 65 from Curriston [2]. The reason for this repetition was to ensure that the blades had reached a well optimized solution. Other methods are proposed to end the algorithm early, but convergence is not always guaranteed with those methods and will not be explored in this project.

3.4.2 Mutation Section

ES is very capable of moving out of a local optimum due to its mutation operator, which is why it was chosen. The most commonly used function to update the mutation is the one-fifth success rule, which was previously discussed. The utility of this method is that if the solution is

converging in a specific search space then the mutation operator will start increasing to diversify the search space in hopes of obtaining a better solution.

The mutation operator has now been defined. The next question is which parameter is going to be mutated. Since this project is in the inverse design phase, we are seeking to optimize the objective functions by mutating the geometry. Since, the geometry was defined by the CST method, the parameters that are going to be mutated are the Bernstein Coefficients. The leading and trailing edge shape parameters were chosen not to be mutated because it introduced too much variable space and would cause the optimizer to take too long to converge with little premise for improved performance. Also, the Bernstein Coefficients can alter the shape of the leading and trailing edge, so the leading and trailing edges are going to be mutated anyways, just not by the shape parameters. Since there are five Bernstein Coefficients for both the suction and pressure side, there are a total of ten mutable parameters. However, design constraints were placed on the blade to ensure a feasible blade. First, the pressure side trailing edge Bernstein Coefficient (A5) was kept constant, so that it would meet the suction side with a continuous curvature. Second, the pressure side Bernstein Coefficient (A2) was kept constant, so that again a continuous curvature was enforced on the blade. There are a total of eight parameters that are being mutated, which will then be checked to ensure that mutated airfoil is a feasible blade acceptable for analysis.

3.4.3 Feasibility

When the blades are mutated, caution must be taken to ensure they are feasible. Blades which are not feasible are likely to have reduced performance and will possibly diverge when being passed to the grid meshing tool or grid CFD analyzer. So, a few simple checks are put into

place to make sure the blades meet feasibility criteria. First, a check is made to ensure blade coordinates from the suction and pressure side have not crossed each other, such as in Figure 7. Second, the arclength to area ratio is checked to ensure that blade cannot get to big or too small. A full structural analysis is outside of the scope of this project and more schemes which utilize a structural analysis can be found in research articles. So, if the blade gets too big then that increases weight and if the blade gets too small, then rotordynamic issues could occur such as high vibration. For all three blades the surface arc length to area ratio could change up to twenty percent.

Chapter 4

CFD Analysis

During application of the ES algorithm, the blades are evaluated using CFD. A sample case is shown in Figure 15 This chapter will provide a brief description of the CFD method and will include a summarized table of initial parameters such as total inlet pressure and temperature. Because this project is not a pure Computational Fluid Dynamics project, the method used to solve the blades will be mentioned in short descriptions and more can be found from the user's manual for both CFD tools. As mentioned earlier, the grid generator tool used was GRAPE [4], and the grid analyzer is RVCQ3D [7]. Also, discussed in this chapter is the objective functions used to rank the blades.

4.1 GRAPE

Using GRAPE, two-dimensional turbomachinery blades and isolated airfoils can be generated. GRAPE can produce O or C type grids for analysis and examples are included for reference [4]. Inner and outer boundary points are specified and then points are solved algebraically. Those points are then smoothed by Poisson's Equation. For the turbine analysis, 256 grids in the streamwise directions are used and in the blade to blade direction 45 grids are used for a total of 11520 grids for one blade mesh grid. Since the initial Rotor 37 grid was provided by GRAPE, the initial set of parameters were kept, so 311 grids were used in the streamwise direction and 63 grids in the blade to blade direction so a total of 19593 grids for one blade mesh. Figure 16

shows the initial NASA Rotor 37 grid, shows the initial EEE stator 1 grid, and shows the initial EEE rotor 1 grid. Included in Appendix B is the grape input for rotor 37, with excluded coordinates.

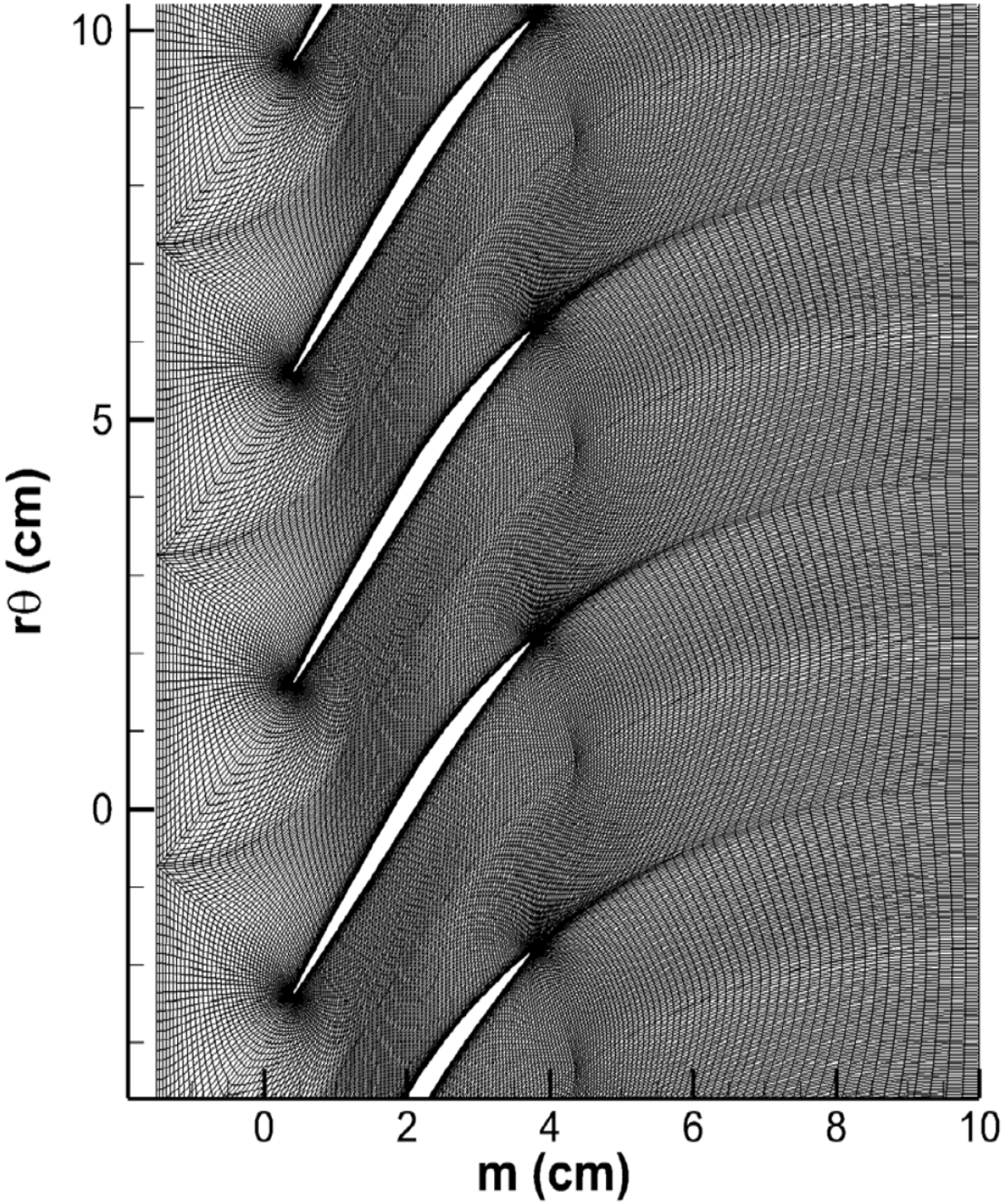

Figure 16. Initial NASA Rotor 37 Grid

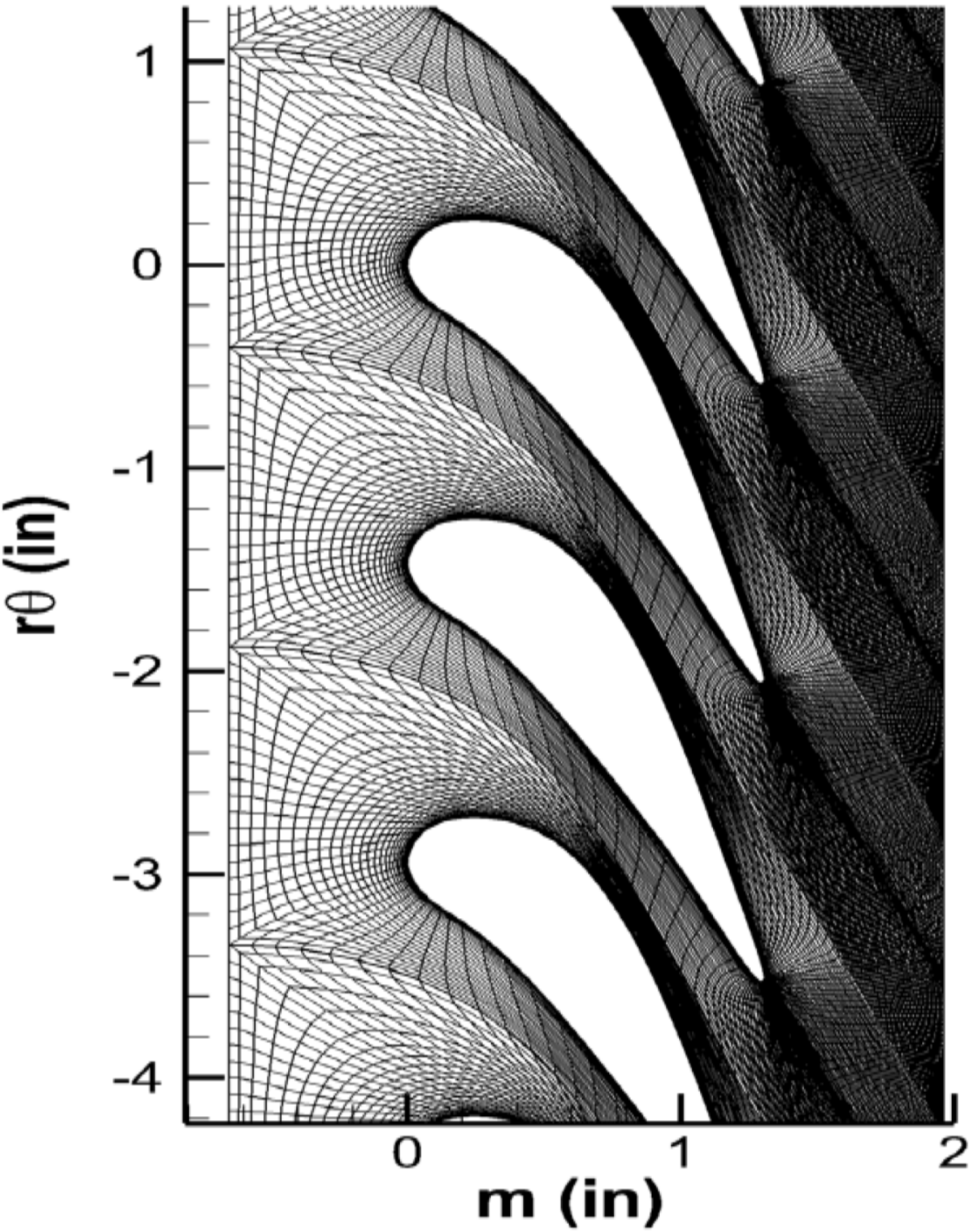

Figure 17. Initial EEE HPT Stator 1 Grid

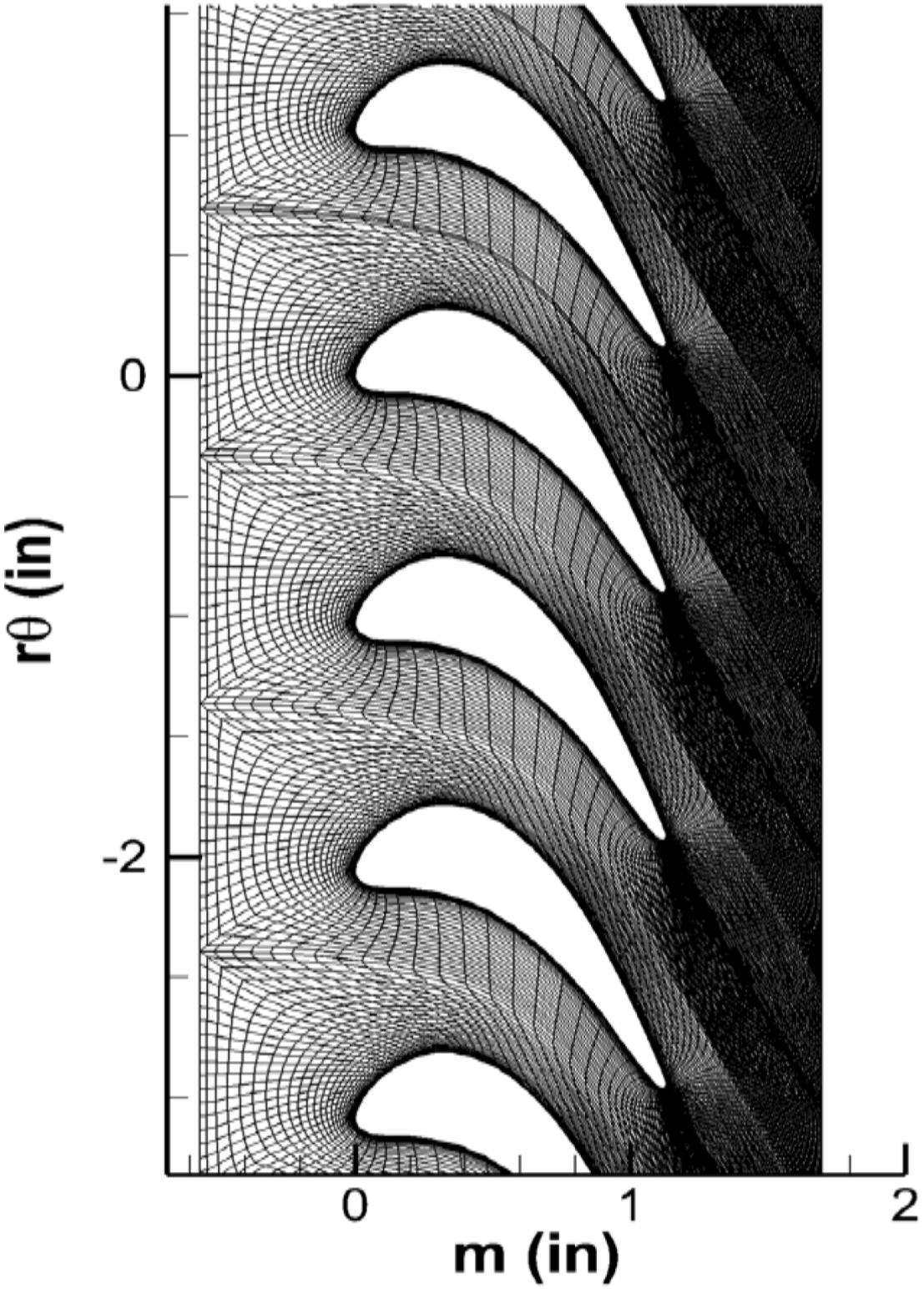

Figure 18. Initial EEE HPT Rotor 1 Grid

4.2 RVCQ3D

RVCQ3D is used to analyze inviscid or viscous quasi-three-dimensional blade-to-blade flows in turbomachinery and it will be summarized and more can be found from the user's manual [7]. It is quasi-three-dimensional because the grids are only two-dimensional, but to include three-dimensional effects rotation, radius change, and stream surface height are implemented in the code. The applications of this code are well implemented for compressor and turbine blades with axial, centrifugal, and mixed flows. The Central Difference Scheme & Artificial Viscosity, AUSM$^+$ Upwind Scheme, and the H-CUSP Upwind Scheme are the available differencing schemes used to solve the thin-layer Navier-Stokes Equations on a blade-to-blade surface of revolution. Included are four turbulent models: the Baldwin-Lomax model; the Cebeci-Smith model; the baseline Wilcox κ-ω model; and the low Reynolds Number Wilcox κ-ω model with transition effects. To converge to a steady-state solution, an explicit multistage Runge-Kutta scheme is used. Once the grids are generated from GRAPE, they are passed to RVCQ3D for analysis and the output data is then used to obtain the values for fitness functions.

4.2.1 EEE HPT Stator/Rotor 1 & Rotor 37

For both the turbine stator and rotor, similar RVCQ3D input files were used. The AUSM$^+$ Wilcox κ-ω model with transition effects was used to model heat effects across both the blades. Also, the boundary conditions used for the EEE HPT Stage 1 can be found on the NASA Technical Report Server [30]. Appendix C shows the input for the Rotor 37 case with excluded stream tube geometry. Like the turbine case, Rotor 37 instead used the H-CUSP method with the same turbulence modeling. The H-CUSP method was used instead because it is better at capturing the

shocks on the blade, which was important for this blade. Shown in the following figures are the initial pressure and Mach Number contours for each blade and shows some of the initial geometry and flow field parameters.

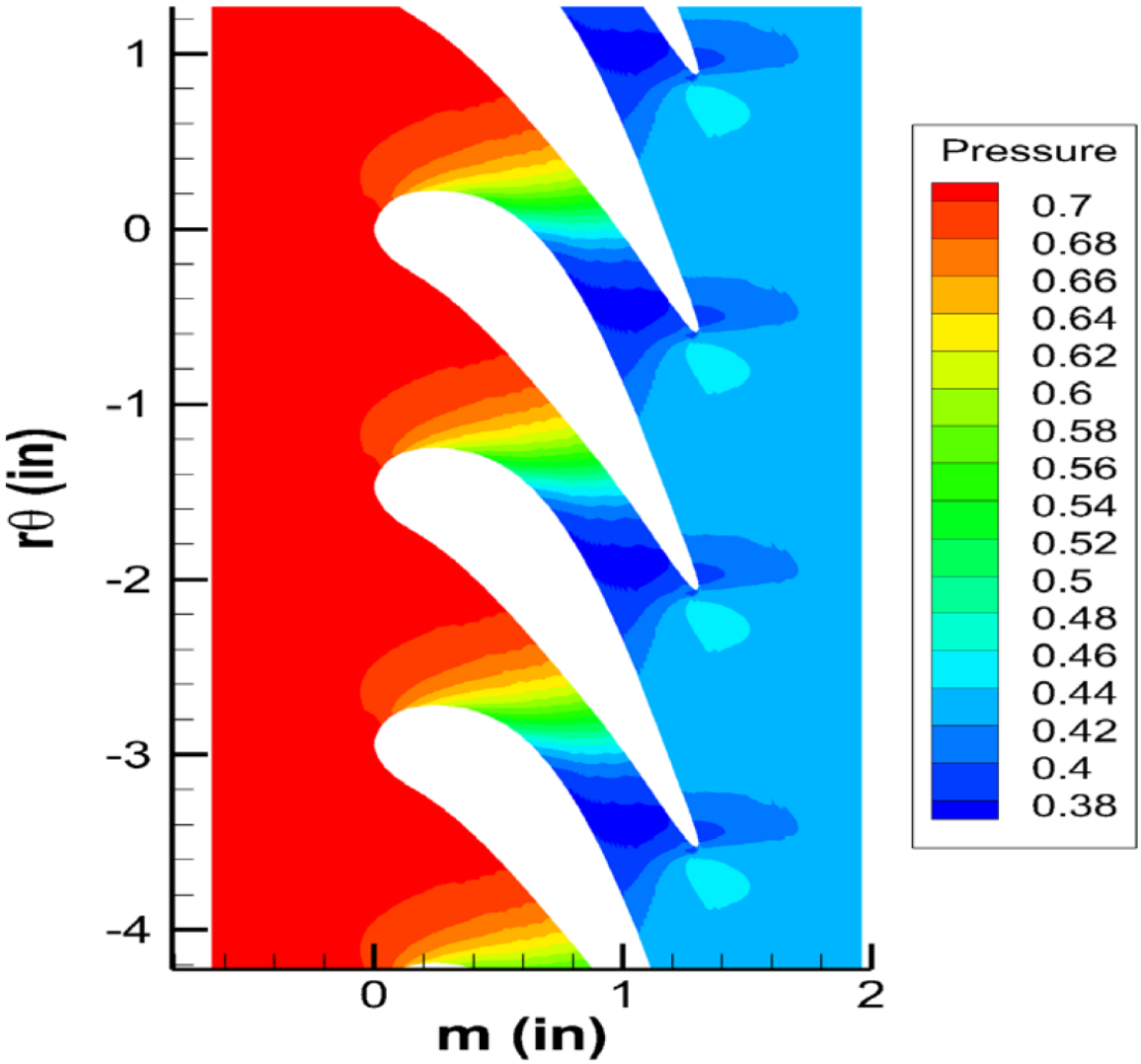

Figure 19. EEE Stator Pressure Flow Field

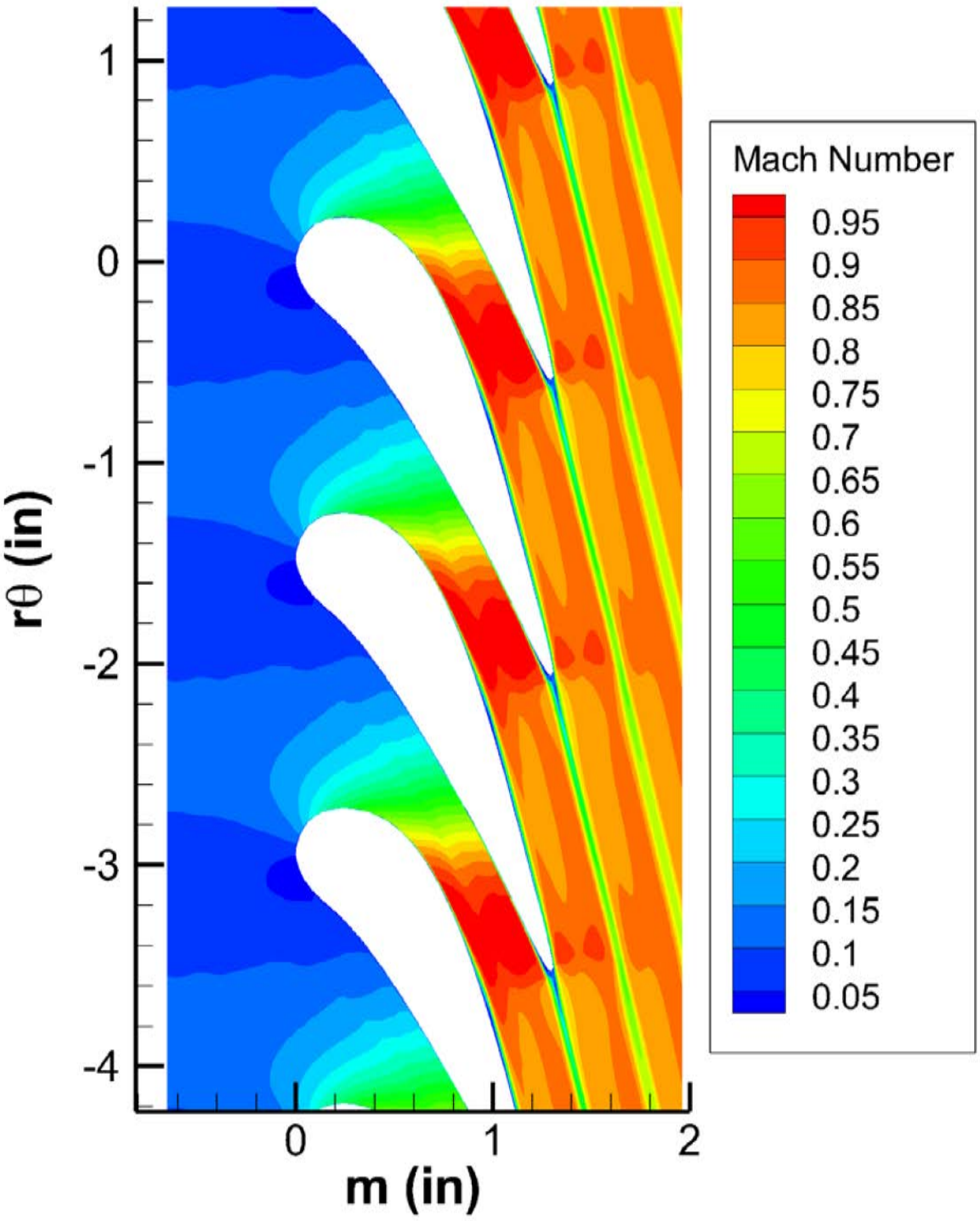

Figure 20. EEE Stator Mach Number Flow Field

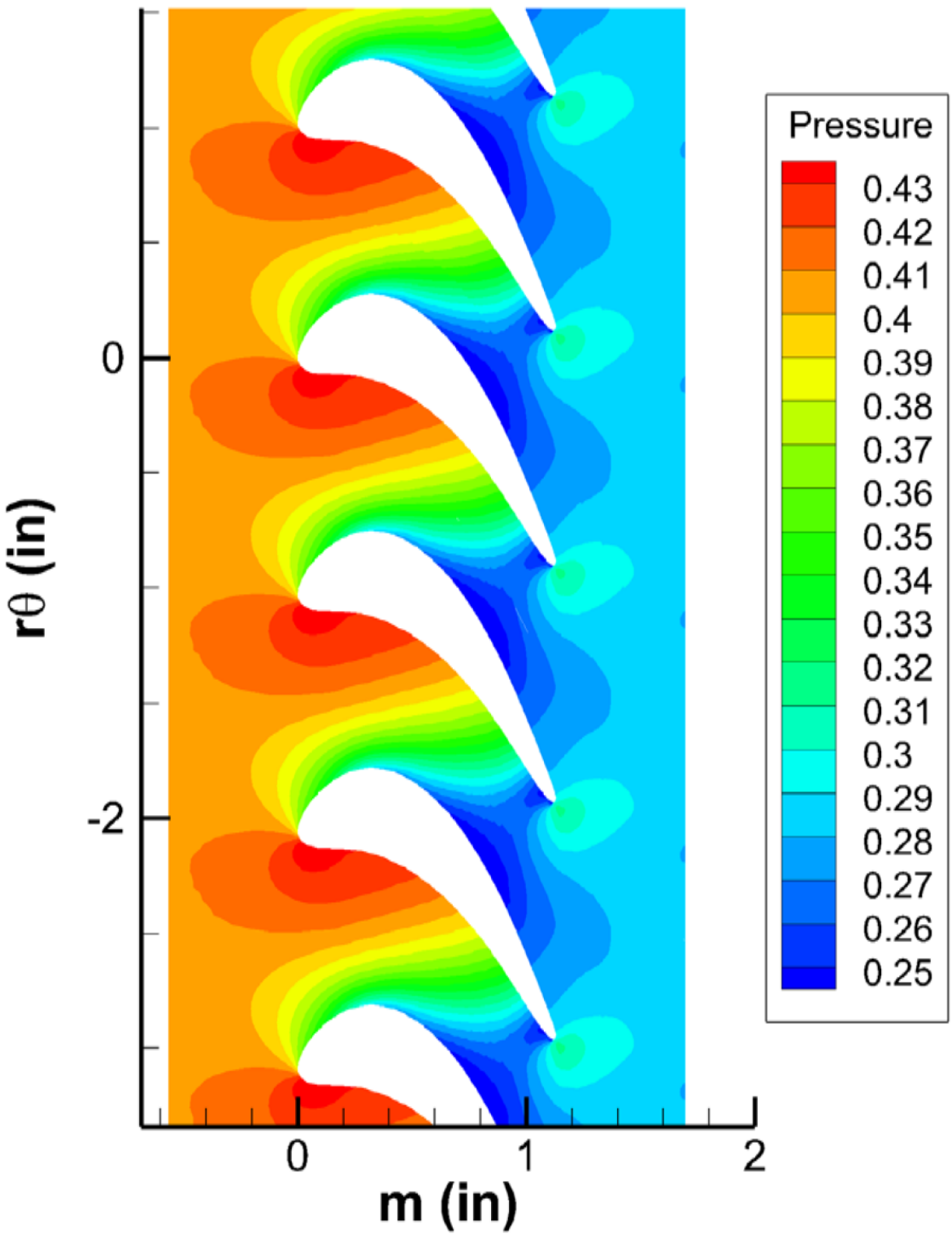

Figure 21. EEE Rotor Pressure Flow Field

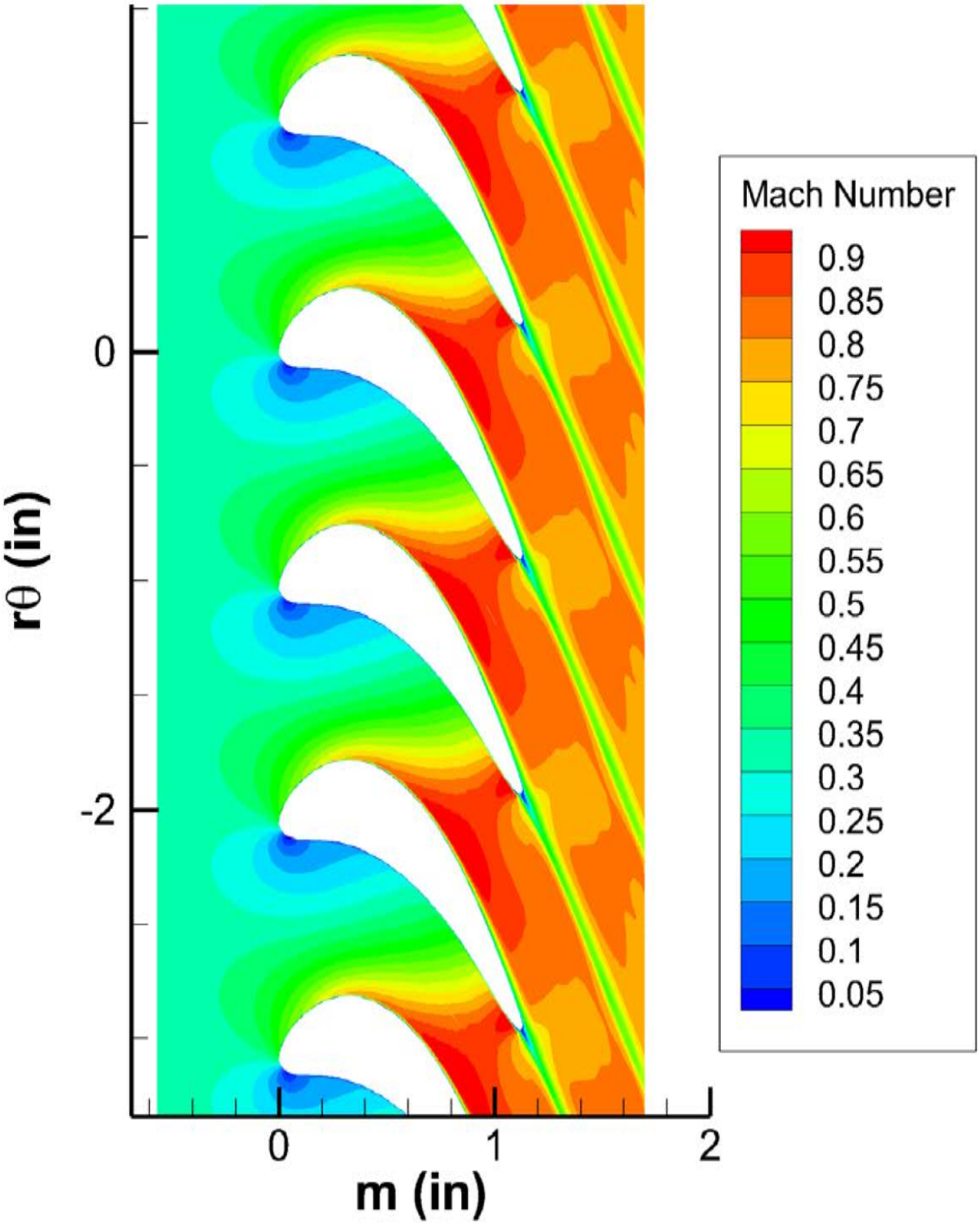

Figure 22. EEE Rotor Mach Number Flow Field

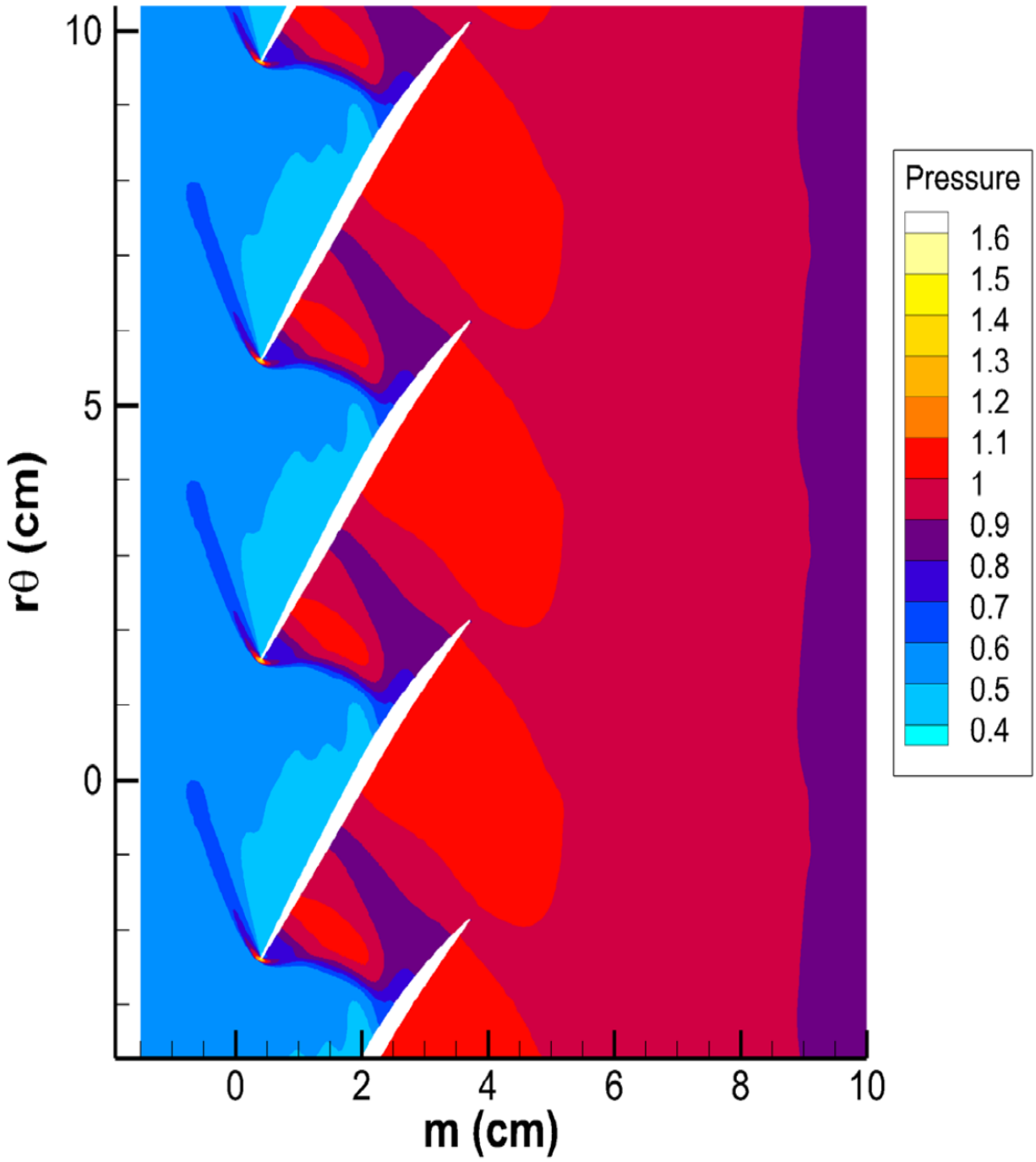

Figure 23. NASA Rotor 37 Pressure Flow Field

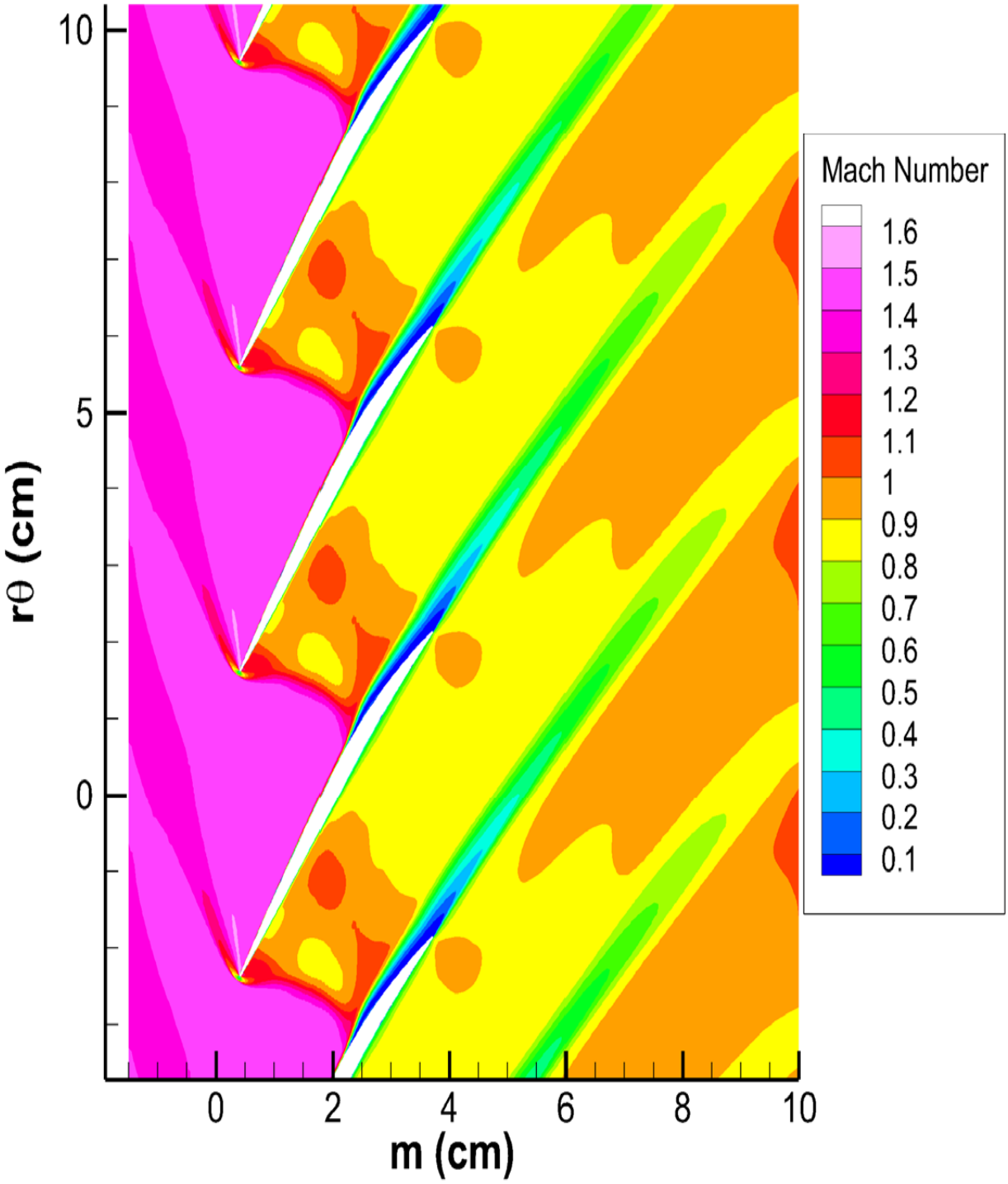

Figure 24. NASA Rotor 37 Mach Number Flow Field

Table 4. Initial Blade Geometry & Flow Field Parameters

Blade	Parameter	Inlet-absolute	Exit-absolute	Inlet-relative	Exit-relative
EEE Stator	α (Degrees)	0.000	-79.475	0.000	-79.475
	$P_0/P_{0,in}$	1.000	0.939	1.000	0.939
	$T_0/T_{0,in}$	1.000	1.001	1.000	1.001
	Mach No.	0.098	0.827	0.098	0.827
EEE Rotor	α (Degrees)	75.116	-14.500	45.937	-66.748
	$P_0/P_{0,in}$	0.94	0.429	0.615	0.596
	$T_0/T_{0,in}$	0.995	0.802	0.881	0.881
	Mach No.	0.874	0.317	0.323	0.778
Rotor 37	α (Degrees)	0.000	-34.931	65.530	40.119
	$P_0/P_{0,in}$	1.000	2.050	2.509	2.207
	$T_0/T_{0,in}$	1.000	1.257	1.301	1.284
	Mach No.	0.576	0.909	1.391	0.975

4.3 Objective Functions

The objective or fitness functions are used to rank the offspring for the optimization scheme. In this project they are based on improving the turbine and compressor section. Therefore, the objective functions are reflective of fundamental turbomachinery characteristics. The fundamental aspect for turbines are to generate power, specifically for the compressor and other engine components since the EEE is a jet engine. The fundamental aspect of the compressor is to increase the inlet pressure to a very high pressure; thus, the compressor requires work. A simple analysis based on the Euler Turbine Equation will be utilized for the turbine optimization scheme.

Because of the limitless number of parameters that can be optimized and due to time constraints, only a few parameters will be optimized. Also, not included in the optimizer is a rotordynamic analysis and it was assumed that the feasibility check would ensure structural integrity.

4.3.1 Turbine Objective Functions

Because the rotors of a turbine require a large pressure force to turn the shaft, it is the goal of the turbine scheme to increase the amount of work available to the engine. Therefore, the parameters which are optimized will be related to pressure and tangential momentum. Since the EEE turbine stage starts with a stator to turn the flow into the rotor, the first optimization scheme will be applied to the stator then the rotor. The problem with the stator being first is that there is pressure loss associated with having to turn the flow, which is necessary for the rotor to have a controlled applied force. So, the first objective function for the stator is minimizing pressure loss, shown in Eq. (4.1) as the pressure ratio to maximize the exit pressure resulting in a minimum pressure loss. Also, in Eq. (4.2), the tangential momentum is maximized from the stator so that the rotor has a higher available momentum speed to produce power. The mass flow and blade speed are constant, and radius barely changes so these terms have been neglected in determining max power. To measure the performance of the entire stage, the total-to-total efficiency, Eq. (4.3), will be used for the rotor case and is normalized to make the objective function in Eq. (4.4). Eq.(4.2) is multiplied to both Eq.'s (4.1) & (4.4). To include a squared effect for both cases, Eq.'s (4.1) & (4.4) are squared when multiplied by Eq. (4.2) to make the total objective functions.

$$OBJ_{1,S} = 1 - \overline{\omega} = \frac{P_{0.EX}}{P_{0.IN}} \tag{4.1}$$

$$OBJ_2 = \left| C_{\theta,EX} - C_{\theta,IN} \right| \tag{4.2}$$

$$\eta_{t-t} = \frac{1 - \frac{T_{0,EX}}{T_{0,IN}}}{1 - \left(\frac{P_{0,EX}}{P_{0,IN}} \right)^{\frac{\gamma-1}{\gamma}}} \tag{4.3}$$

$$OBJ_{1,R} = \frac{\eta_{t-t,NEW}}{\eta_{t-t,INITIAL}} \tag{4.4}$$

Since these parameters are based on aerodynamic principles, which neglect heat, another set of cases will be ran to heat transfer. There will be two cases, which compare the optimized results for improving the aerodynamics and another one that includes aerodynamics and heat. If the heat transfer on the blade is controlled, then the blade can be optimized to accept a higher available temperature. This does not mean that a higher temperature will be the new cruise condition temperature from the combustor, it will simply be a new inlet temperature that keeps the blade at the same temperature as it was before. So, to quantify this temperature into performance, a shaft power ratio equation is derived in the following equations based on inlet conditions. To obtain a new inlet temperature, the heat transfer coefficient will be calculated first. The Stanton Number is calculated in RVCQ3D and can be written in the form of the heat transfer coefficient as shown in Eq. (4.5).

$$St = \frac{h}{\rho_{IN} V_{IN} C_P} \tag{4.5}$$

Assuming the blade temperature and the heat transfer into the blade are constant, a new heat transfer coefficient may be obtained to calculate a new total turbine inlet temperature in Eq. (4.7).

$$q = h\left(T_0 - T_{WALL}\right) \tag{4.6}$$

$$T_{0,NEW} = \frac{h_{NEW}}{h_{INITIAL}}\left(T_{0,INITIAL} - T_{WALL,INITIAL}\right) + T_{WALL,INITIAL} \tag{4.7}$$

An ideal shaft power equation from Flack [18] may then be used to derive a shaft power ratio equation by taking a curve fit analysis in Eq. (4.9). This shaft power ratio is then multiplied to the stator & rotor objective functions for two total objective functions Eq.'s (4.10) & (4.11).

$$\mathrm{P}_{NET,SHAFT} = \dot{m}C_P T_a\left[\frac{T_{0,Turbine}}{T_a}\left(1 - \frac{1}{\tau_{Compressor}}\right) - \left(\tau_{Compressor} - 1\right)\right] \tag{4.8}$$

$$OBJ_3 = \frac{\mathrm{P}_{NEW}}{\mathrm{P}_{INITIAL}} = 1.3216\frac{T_{0,NEW}}{T_{0,INITIAL}} - 0.3216 \tag{4.9}$$

$$OBJ_{STATOR} = OBJ_{1,S}^2 OBJ_2 OBJ_3 \tag{4.10}$$

$$OBJ_{ROTOR} = OBJ_{1,R}^2 OBJ_2 OBJ_3 \tag{4.11}$$

4.3.2 Turbine Penalty Functions

Penalty functions are only used if a certain condition is met, typically a condition which reduces the design performance. So, a value is multiplied to reduce the fitness value, so that the "optimized" blade does not have reduced performances physically. Also, when the optimizer takes

the previous objective functions mentioned, it does not know the blade may have some reduced flow field characteristics. So, the optimizer scheme must be taught to catch reduced performance characteristics as well. The characteristics of interest are the Mach number distribution and diffusion across the blade.

A major aspect of turbine blade design is to ensure that the Mach number is monotonically increasing across the suction side, so that there are no adverse pressure gradients [17]. These adverse pressure gradients, like the one shown on Figure 25 [17], can cause boundary layer buildup and flow separation can occur, which will reduce performance. Typically, in turbine blade design this is not a big issue because blades are easily designed to have monotonically increasing velocity. However, the optimizer needs to know that this is a dominating characteristic of turbine blade design because the optimizer does not know that adverse pressure gradients are a bad characteristic to have. So, to ensure that the Mach number is monotonically increasing across most of the blade, a strict penalty value of 0.25 is multiplied is to the total objective function if the flow is not monotonically increasing. Also, the velocity is checked to ensure it does not decrease before the

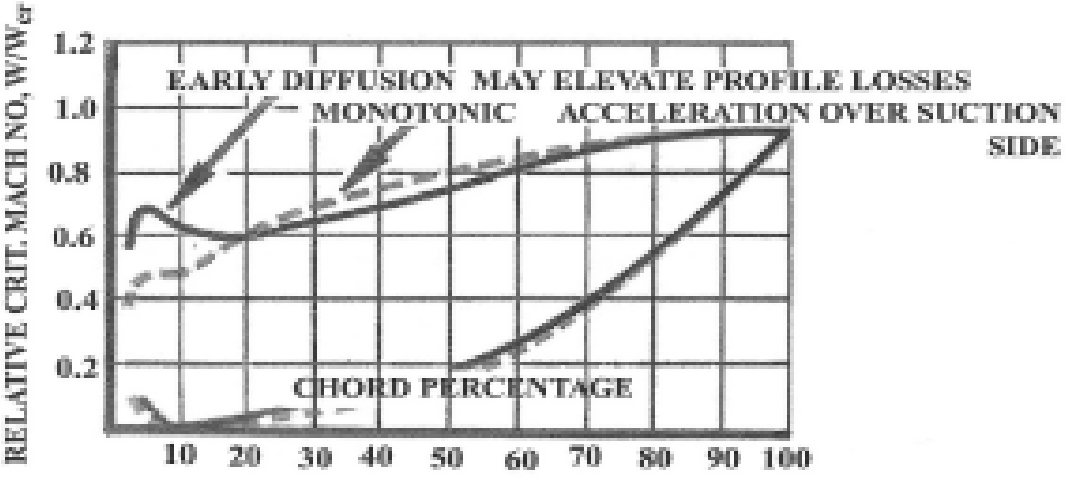

Figure 25. Adverse Pressure Gradient from a Non-Monotonically Increasing Mach Number

throat section and if it decreases more than 15 percent of the exit Mach number a penalty function is applied.

The diffusion parameter is also useful for checking the flow of the blade, especially the suction side of the blade to ensure the uncovered turning angle is not too large. From Baskharone [17], if the diffusion exceeds 0.25 then a penalty is also applied. Eq. (4.12) & (4.13) show the stator and rotor diffusion, respectively, and Eq. (4.14) is the penalty equation if the diffusion exceeds 0.25.

$$\bar{\lambda}_{Stator} = \frac{\left(\frac{P}{P_0}\right)_{EX} - \left(\frac{P}{P_0}\right)_{MAX,V}}{1 - \left(\frac{P}{P_0}\right)_{MAX,V}} \tag{4.12}$$

$$\bar{\lambda}_{Rotor} = \frac{\left(\frac{P}{P_0}\right)_{EX} - \left(\frac{P}{P_0}\right)_{MAX,W}}{1 - \left(\frac{P}{P_0}\right)_{MAX,W}} \tag{4.13}$$

$$PEN = 1 - (\bar{\lambda} - 0.25) \tag{4.14}$$

4.3.3 Compressor Objective Functions

Several studies to optimize compressors use similar objective functions. This project will use the two most popular objective functions because they are the most fundamental to compressor aerodynamics. The first one is the pressure ratio, which is shown in Eq. (4.15). Second, the efficiency in Eq. (4.16), which has come a long way in terms of efficiency improvement compared to turbine efficiency. The reason for this is because of the adverse pressure gradient that is inherit

to compressors. Because of the adverse pressure gradients, there is a boundary layer buildup which contributes to flow separation and ultimately, reduced performance. Eq.'s (4.15) & (4.16) are multiplied together to make the final objective function Eq. .

$$OBJ_1 = \pi_C = \frac{P_{0,EX}}{P_{0,IN}} \tag{4.15}$$

$$OBJ_2 = \eta_{ad} = \frac{\left(\frac{P_{0,EX}}{P_{0,IN}}\right)^{\frac{\gamma-1}{\gamma}} - 1}{\frac{T_{0,EX}}{T_{0,IN}} - 1} \tag{4.16}$$

$$OBJ_{ROTOR37} = OBJ_1 OBJ_2 \tag{4.17}$$

4.3.4 Initial Fitness Values

Displayed on Table 5 are the initial objective functions for all three blades and the penalty functions are excluded because they have a value of 1 unless the penalty condition is met. Objective function 2 for the turbine stator and rotor case are displayed unsquared and the rotor is shown is shown unnormalized, so what is displayed is the initial efficiency of the HPT Stage 1.

Table 5. Initial Fitness Values for all Blade Cases

BLADE	OBJ_{Final}	OBJ_1	OBJ_2	OBJ_3

EEE Stator	67.3617	0.93972	76.281	1.00
EEE Rotor	85.4808	92.44	85.48	1.00
Rotor 37	1.8417	0.87797	2.0977	NA

Chapter 5

Optimizer Results

Displayed in this chapter are the results for all the blades. For the turbine, there are two different cases which highlight effects of aerodynamics without heat transfer considerations and one with heat transfer considerations described in 4.3.1 Turbine Objective Functions. Each case has three runs, so there a total of 6 runs for each blade row in the turbine section. Since, thermal considerations are not as important for the compressor 3 runs were completed. Each case uses the same objective function. With optimization it useful to show multiple runs to show proof of convergence. 8 offspring are evaluated each generation and there are 100 generations for a total of 800 CFD evaluations. All the cases are simulated on a 4.0 GHz 8-core processor. Completion time for the turbine rotor & stator case were approximately 7 hours to complete. Completion time for Rotor 37 took approximately 21.4 hours.

5.1 NASA EEE HPT Stator 1 Results

The first set of results to be displayed are the aerodynamic runs without heat transfer considerations. A pressure and tangential momentum increase is expected, and we should be able to see how these parameters change in the flow field. From Figure 26, compared to Figure 20 the Mach number contour increase due to the tangential velocity increasing and the same can be seen in Figure 29 & Figure 31. More importantly, in Figure 27 the pressure loss is decreased across the suction side compared to Figure 19, which increases the amount of pressure force the rotor blade will experience to increase power. Figure 28 & Figure 30 also show a decreased pressure loss across the suctions side.

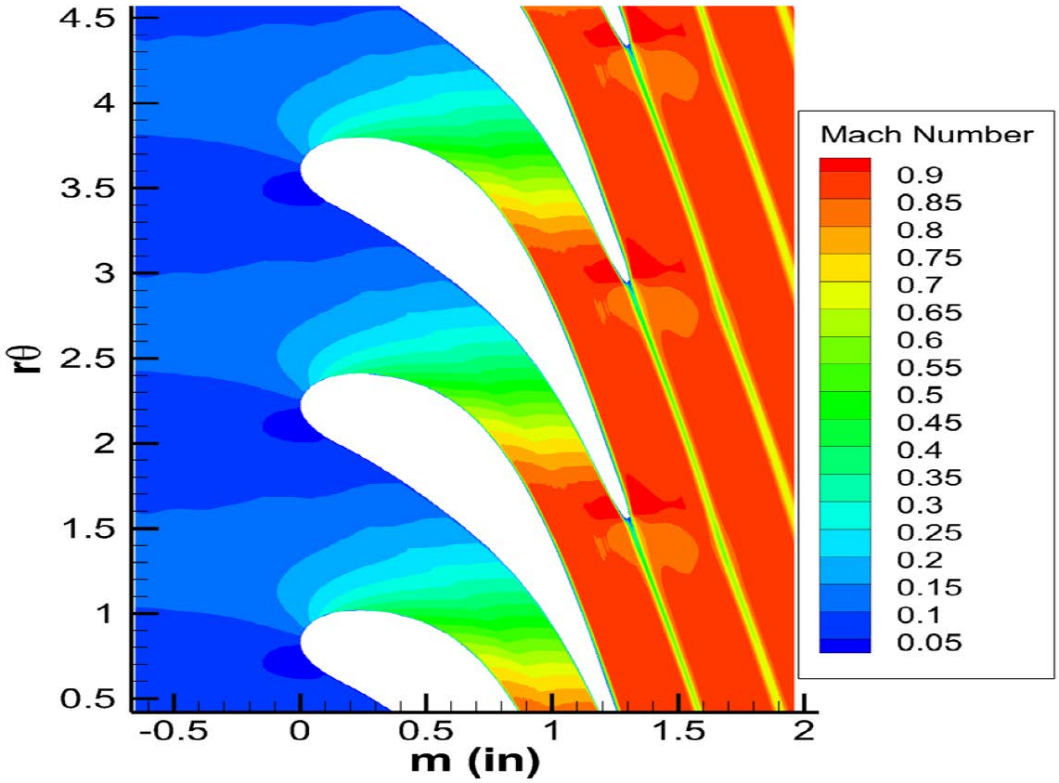

Figure 26. EEE Stator 1 Run 1 Mach No. w/no Heat Considerations

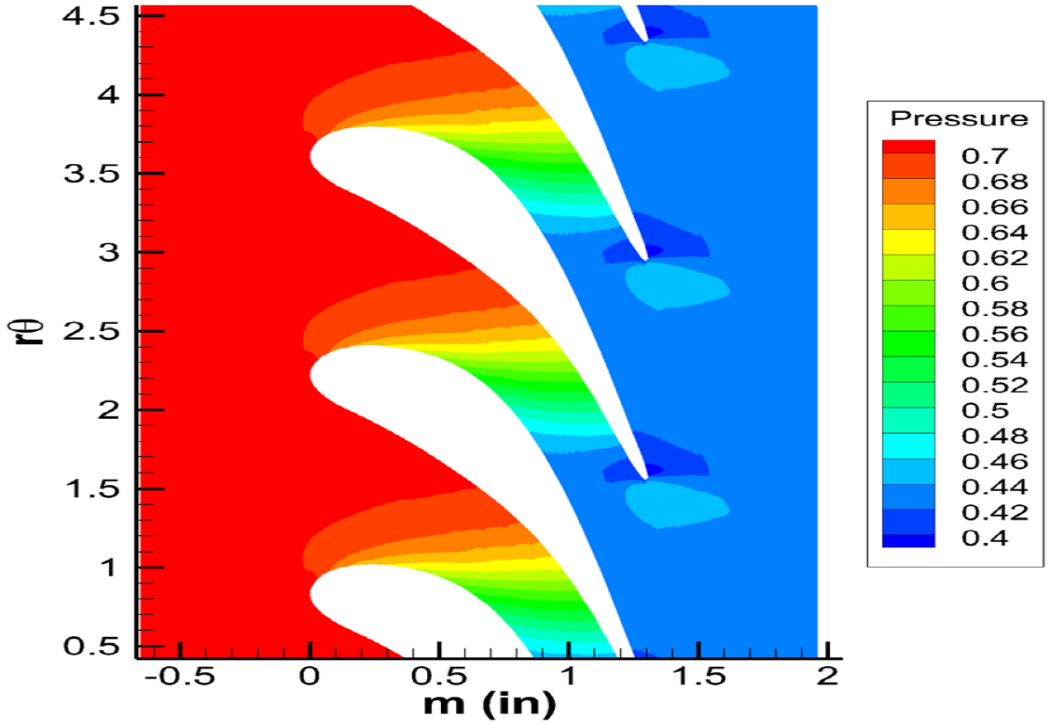

Figure 27. EEE Stator 1 Run 1 Pressure w/no Heat Considerations

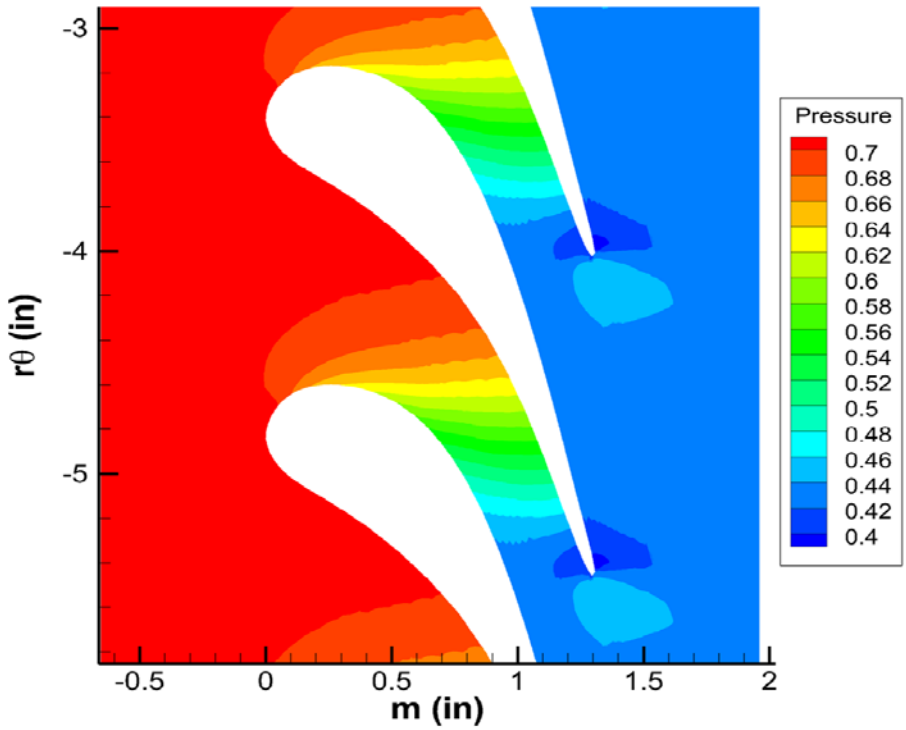

Figure 28. EEE Stator 1 Run 2 Pressure w/no Heat Considerations

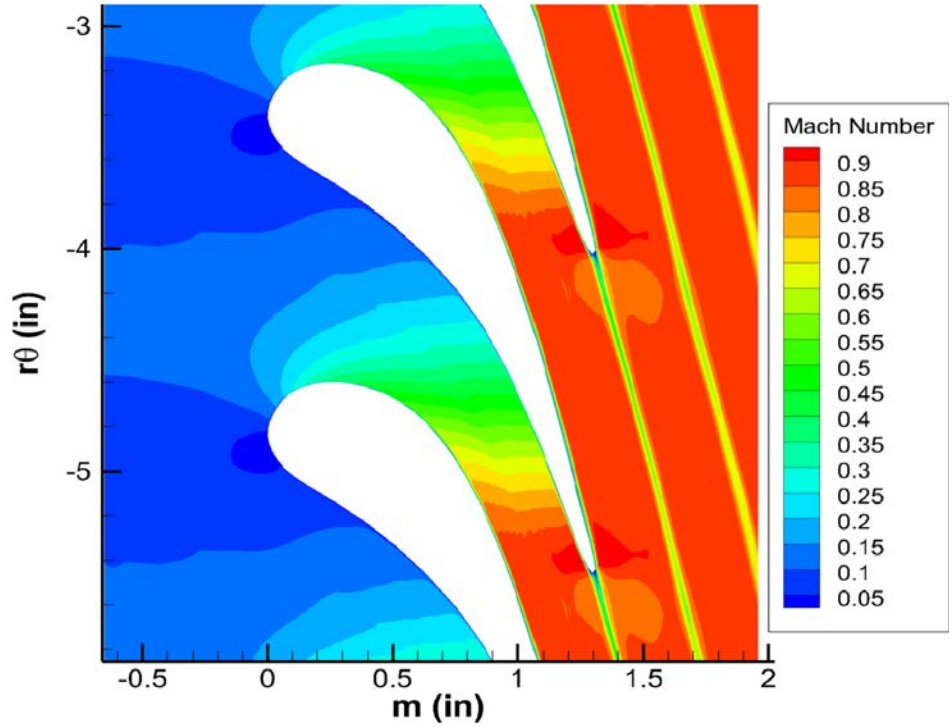

Figure 29. EEE Stator 1 Run 2 Mach No. w/no Heat Considerations

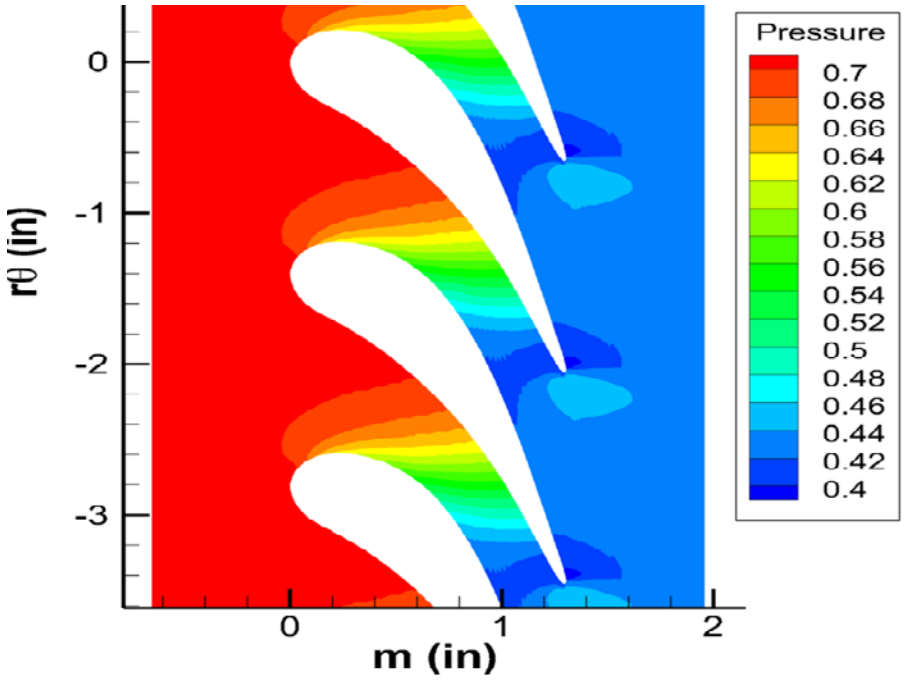

Figure 30. EEE Stator 1 Run 3 Pressure w/no Heat Considerations

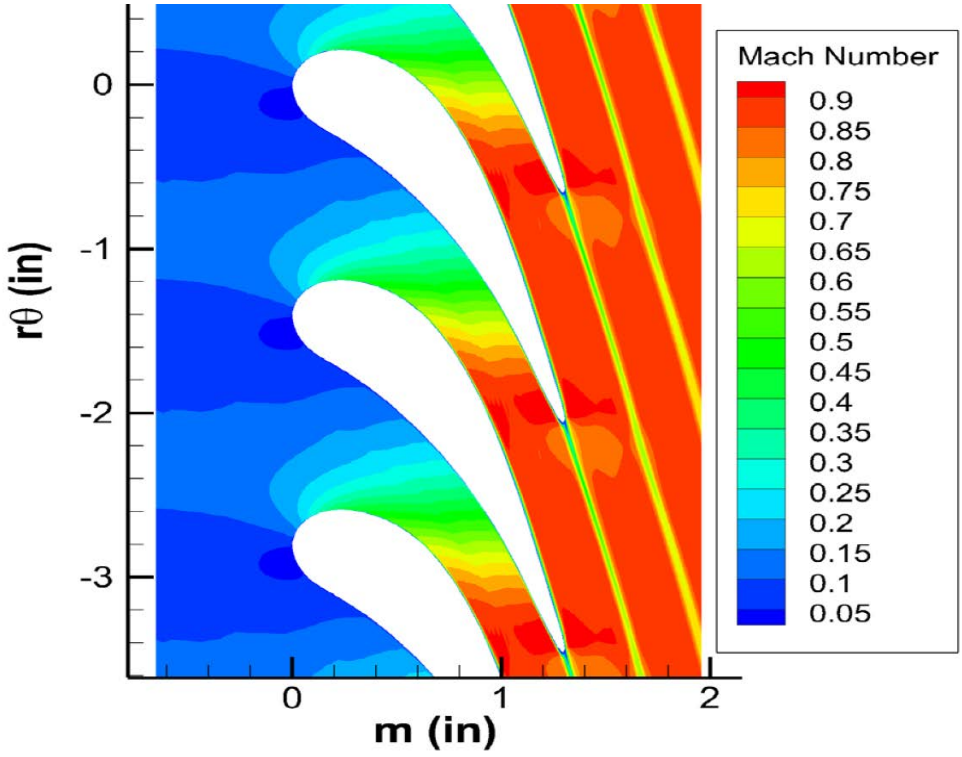

Figure 31. EEE Stator 1 Run 3 Mach No. w/no Heat Considerations

On Table 6 shows the optimized objective functions compared to the initial blade. Run 2 shows that it was the best optimization and the parameters were increased by 2.58% & 2.68% for OBJ(1) & OBJ(2), respectively, which increased the overall fitness value by 8.65%.

Table 6. EEE Stator 1 w/no Heat Considerations Objective Function Values

Case	OBJ_Final	OBJ(1)	OBJ(2)
EEE Stator	67.3617	0.93972	76.281
Run 1	73.068211	0.96493	78.476
Run 2	73.188693	0.96543	78.524
Run 3	72.472513	0.96232	78.259

Figure 32 shows how the blade shapes changed and the most noticeable change is the pressure side allowing a smooth transition between the throat section, thus allowing the pressure loss to be reduced. The leading edge also did change a bit and it can be seen that it keeps the elliptic shape, however it is not a uniform elliptic shape on the suction and pressure side. The elliptic shape stays because the optimization was configured for decreasing the pressure loss so the blade LE stays “sharp”, instead of turning more blunt shaped. Table 7 shows Run 2, which was the best run, and how the flow field parameters changed due to optimizing the blade. Because he pressure ratio & Mach number increased, this proves that the rotor will be able to provide more shaft power.

Table 7. EEE Stator 1 w/no Heat Considerations Run 2 Parameter Changes

Blade	Parameter	Inlet-abs	Exit-abs
EEE Stator	α (Degrees)	0.000	-79.475
	$P_0/P_{0,in}$	1.000	0.939
	Mach Number	0.098	0.827
Run 2	α (Degrees)	0.000	-80.069
	$P_0/P_{0,in}$	1.000	0.965

	Mach Number	0.0958	0.853

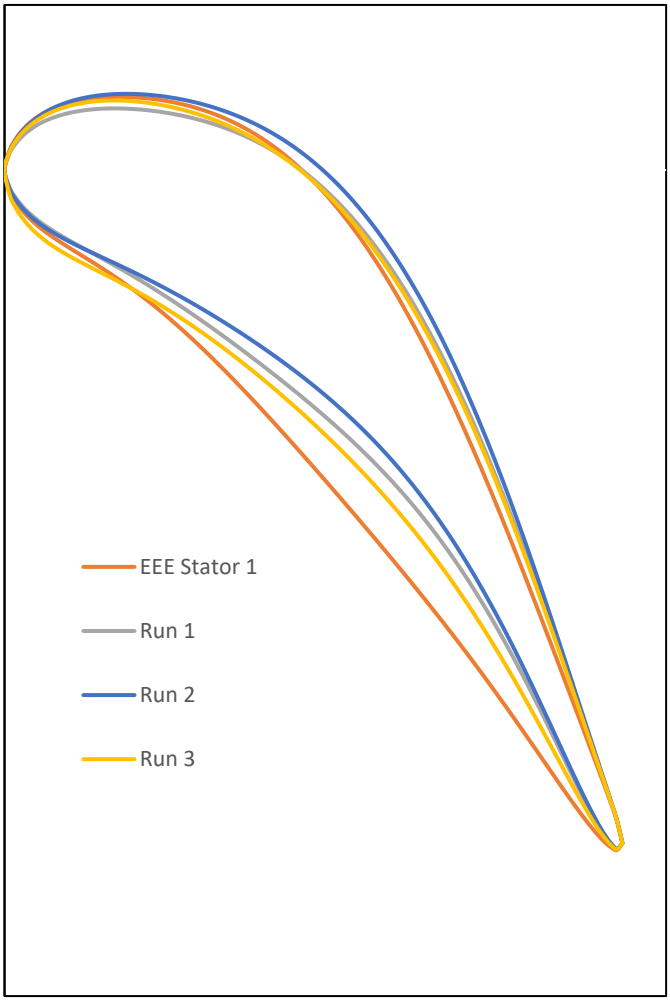

Figure 32. Comparison of Final Stator Geometries w/no Heat Considerations

Next, heat considerations are shown to include how the blade shape and flow field parameters will change. From Curriston & Thorn, it is expected that the LE will become more blunt shaped to accept a higher temperature. Because the other objective functions are also included, it should be noted that the same pressure loss and tangential momentum is not expected.

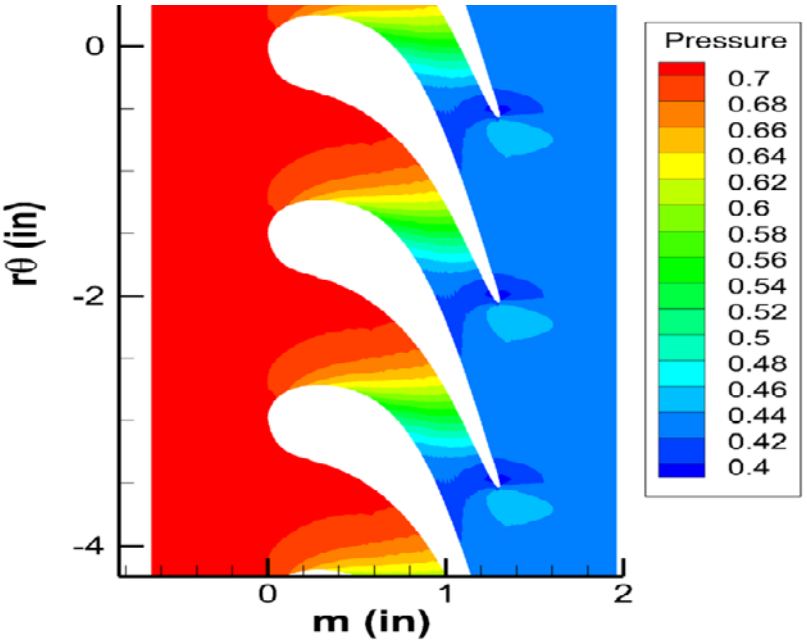

Figure 33. EEE Stator 1 Run 1 Pressure with Heat Considerations

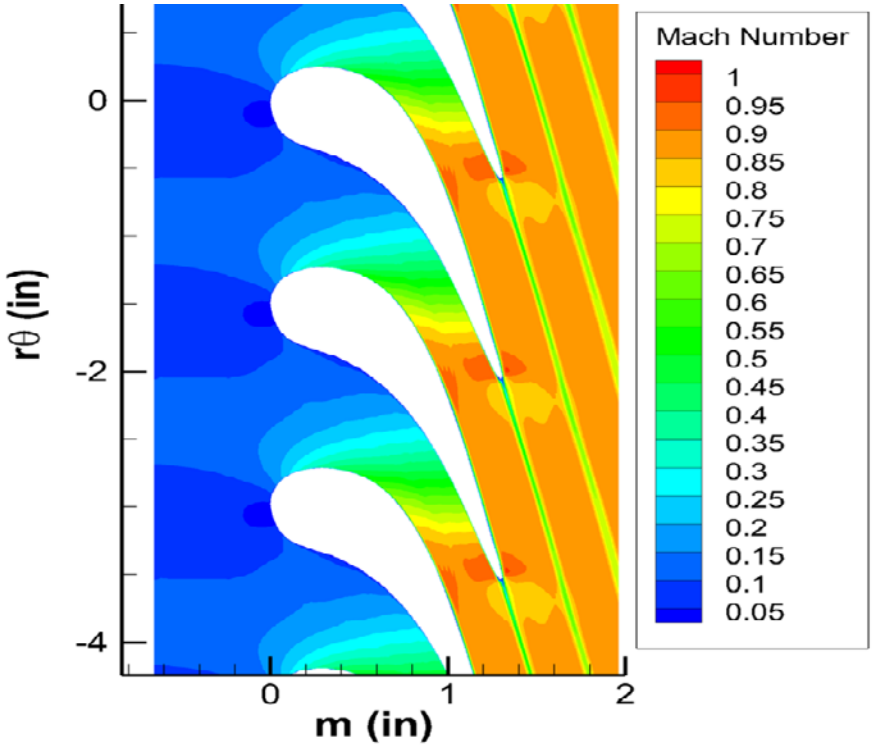

Figure 34. EEE Stator 1 Run 1 Mach No. with Heat Considerations

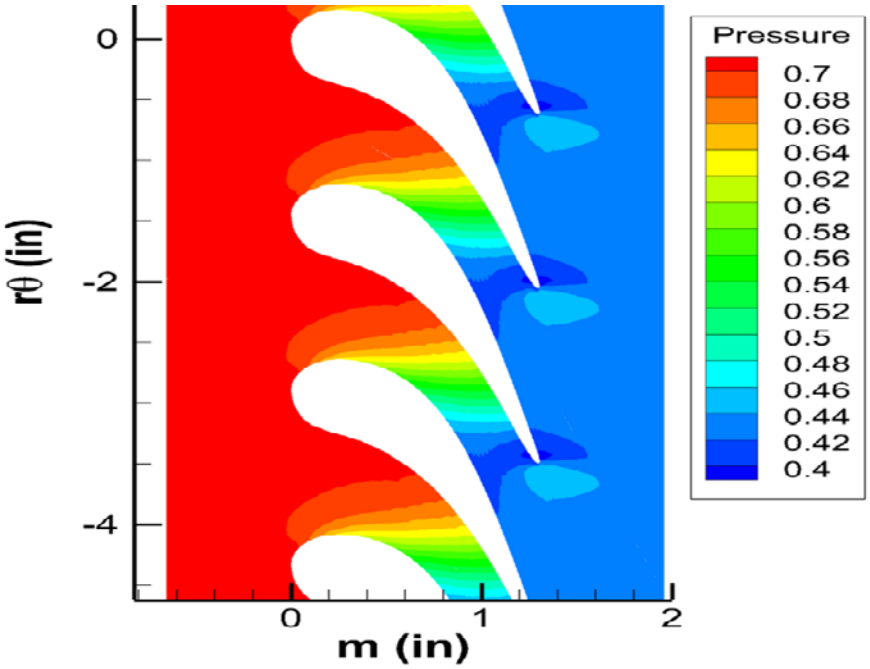

Figure 35. EEE Stator 1 Run 2 Pressure w/Heat Considerations

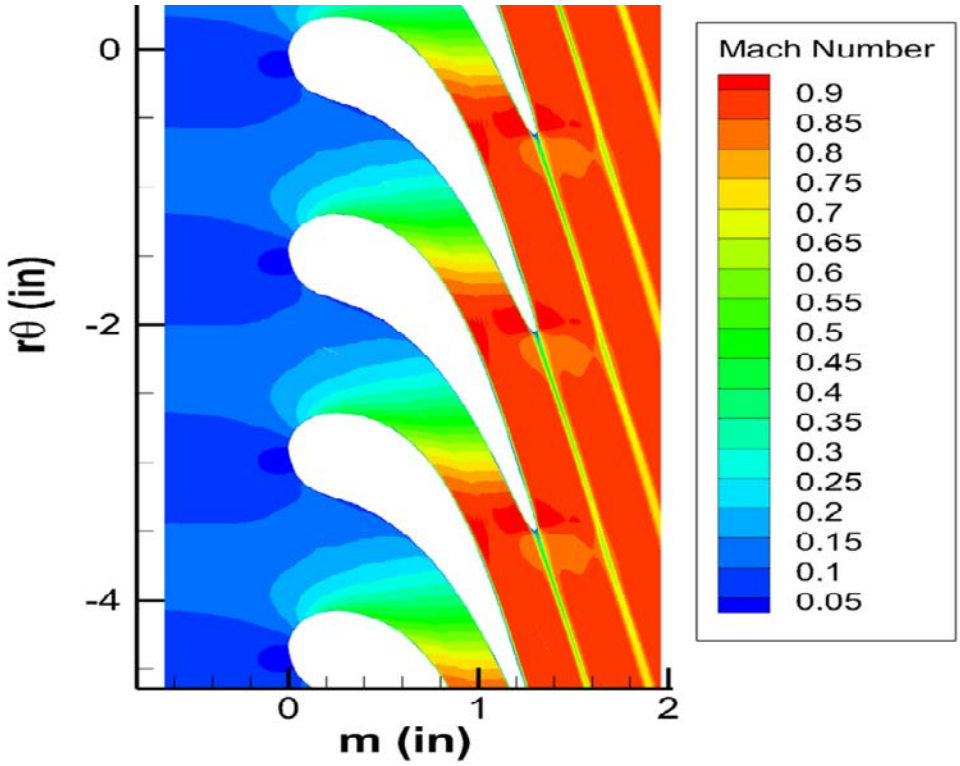

Figure 36. EEE Stator 1 Run 2 Mach No. w/Heat Considerations

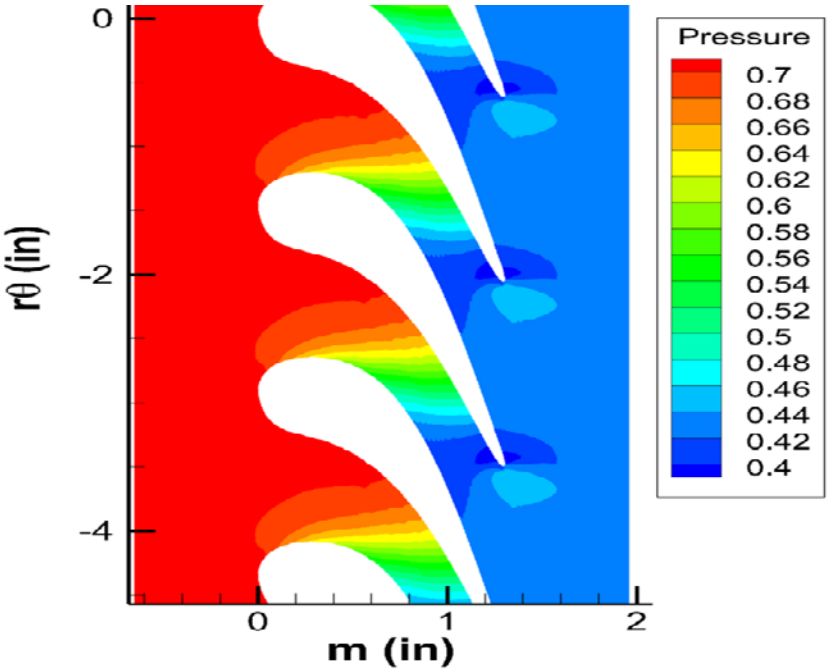

Figure 37. EEE Stator 1 Run 3 Pressure w/Heat Considerations

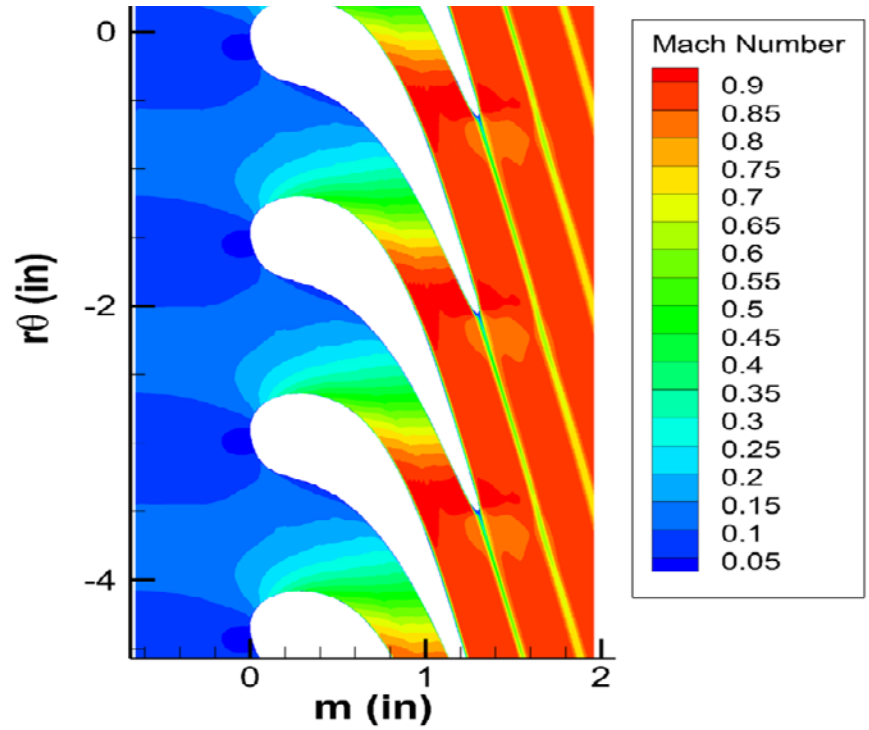

Figure 38. EEE Stator 1 Run 3 Mach No. w/Heat Considerations

From Figure 33 to Figure 37, it is shown that the pressure loss is decreased, but did not decrease as much because there are more pockets of lower pressure on the suction side. However, clearly the LE changes significantly compared to the stator blades with no heat considerations. Therefore, the blade was able to reduce the heat transfer coefficient across the blade. To show this effect, Table 8 shows the overall fitness values and included is the ratio the max allowable turbine inlet temperature can increase without increasing the temperature of the blade.

Table 8. EEE Stator 1 Fitness Values with Heat Considerations

Case	OBJ_Final	OBJ(1)	OBJ(2)	OBJ(3)	$T_{0,new}/T_{0,old}$
Initial	67.2532	0.9399	76.117	1.0000	1.0000
Run 1	73.5420	0.9633	78.168	1.0138	1.0209
Run 2	73.2404	0.9635	78.175	1.0090	1.0136
Run 3	72.9016	0.9607	77.948	1.0132	1.0200

From Figure 33 & Figure 34, which were the best cases, the LE shape became blunt shaped to increase the allowable temperature. Table 8 does show an increase in the fitness value compared to Table 6, but if OBJ(3) is neglected than Run 1 is barely better than the lowest case from Table 6. This is very important to note, because it shows that the more parameters are sought to be increased there must be compromise between the other variables because individually, all the parameters cannot be optimized to their max. Turbine designers often have to neglect certain parameters to achieve a max setting for another parameter. Also from Figure 39, we can see the effect of optimizing for shaft work causes the LE to become more blunt shaped and is even more parabolic shaped compared to the initial EEE blade. But we still see some of the same features like the increased curvature resulting in a decreased pressure loss and increase in tangential momentum.

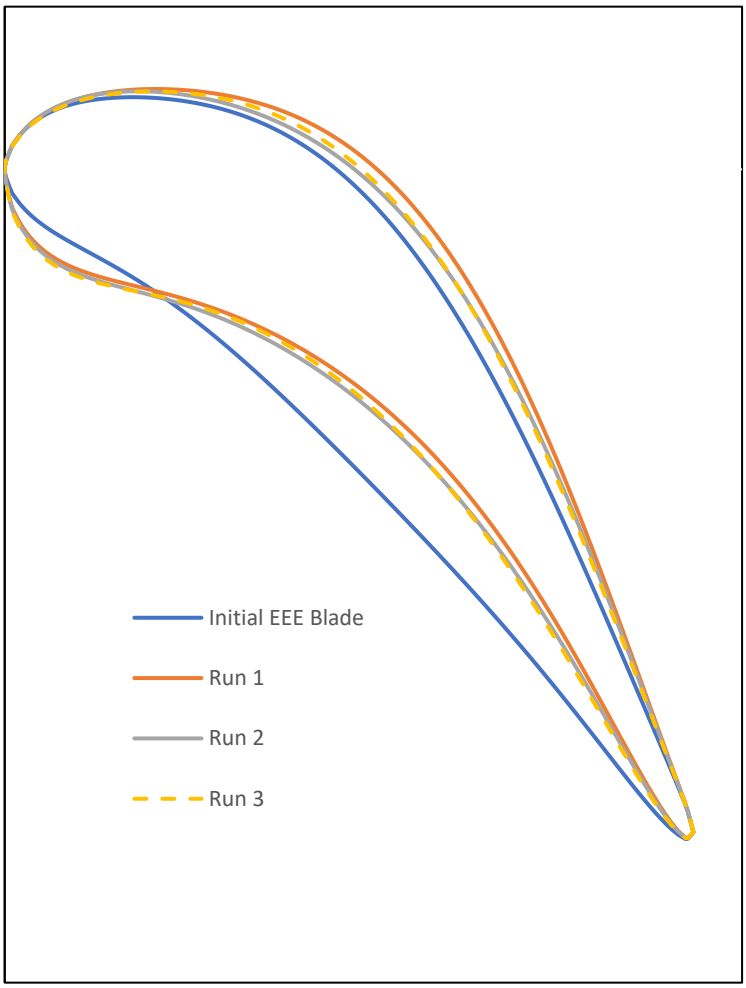

Figure 39. Comparison of Final Stator Geometries with Heat Considerations

5.2 NASA EEE HPT Rotor 1 Results

Similar results will be seen for the turbine rotor section as well. Since, the efficiency is being optimized for, a pressure increase on the pressure side should be more noticeable compared to the initial blade. Looking at Figure 40, this pressure increase on the pressure side is much more significant than the initial blade. The dark red high pressure is now elongated further down the LE compared to the initial blade where most of the high-pressure region is focused on the LE, as

shown in Figure 21. The high-pressure elongation can also be seen through the Mach number contour on Figure 41. because the Mach number is very low and elongates further down the blade compared to the Mach number from Figure 22, which only has a small bubble region where the Mach number stays low. Also, the geometry of the LE change quite significantly because the pressure side slope increases before curving down to the TE. This is because the absolute flow angle at the LE is 74.2° from the meridional axis, so to capture more of the pressure flow the blade LE increases the curvature on the pressure side. The penalty function also makes sure that the uncovered turning angle is not too large and ensures that the flow does not have a large separation bubble and can be seen on Figure 41. These effects are also very noticeable from the other two cases for Figure 40 to Figure 45.

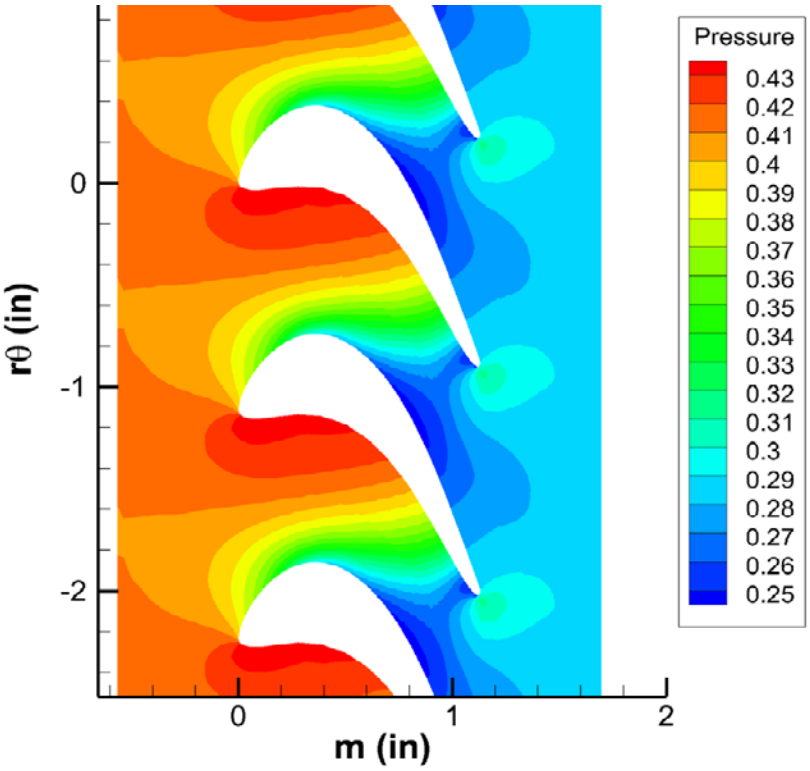

Figure 40. EEE Rotor 1 Run 1 Pressure w/no Heat Considerations

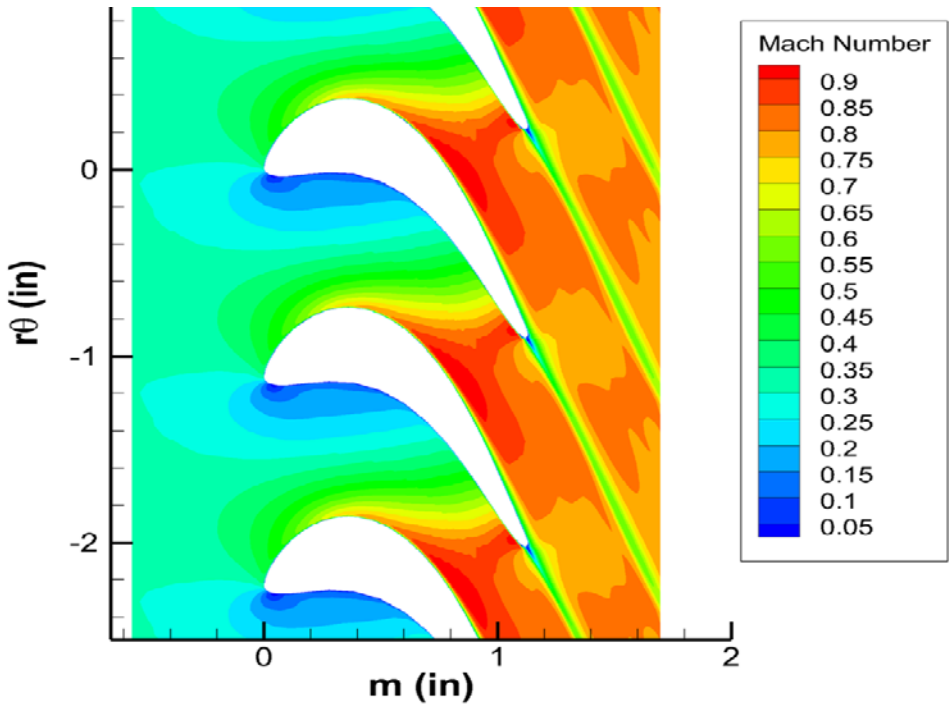

Figure 41. EEE Rotor 1 Run 1 Mach No. w/no Heat Considerations

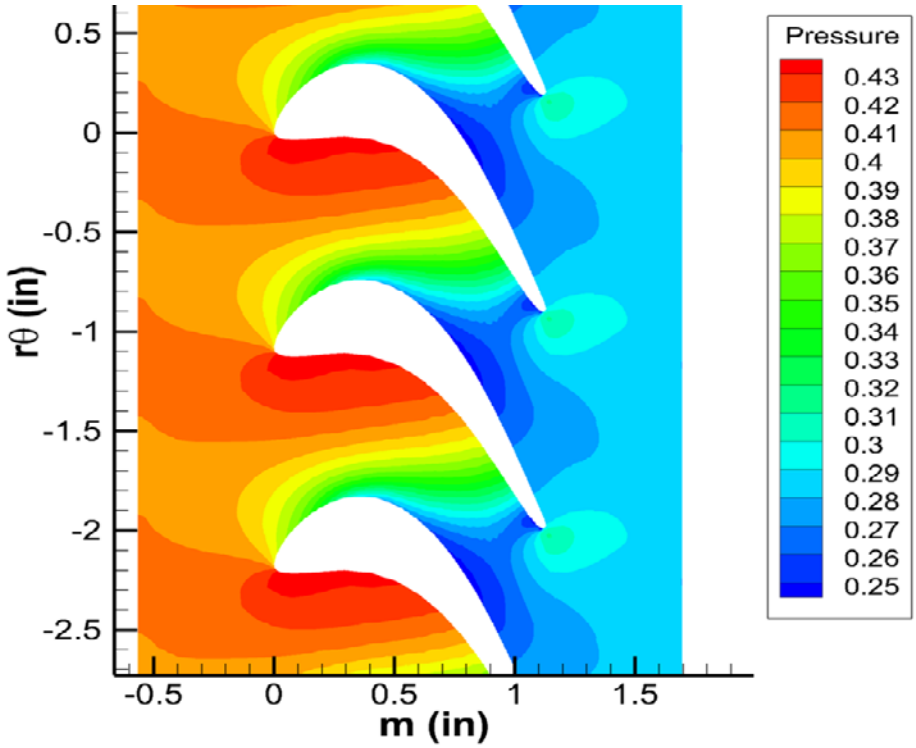

Figure 42. EEE Rotor 1 Run 2 Pressure w/no Heat Considerations

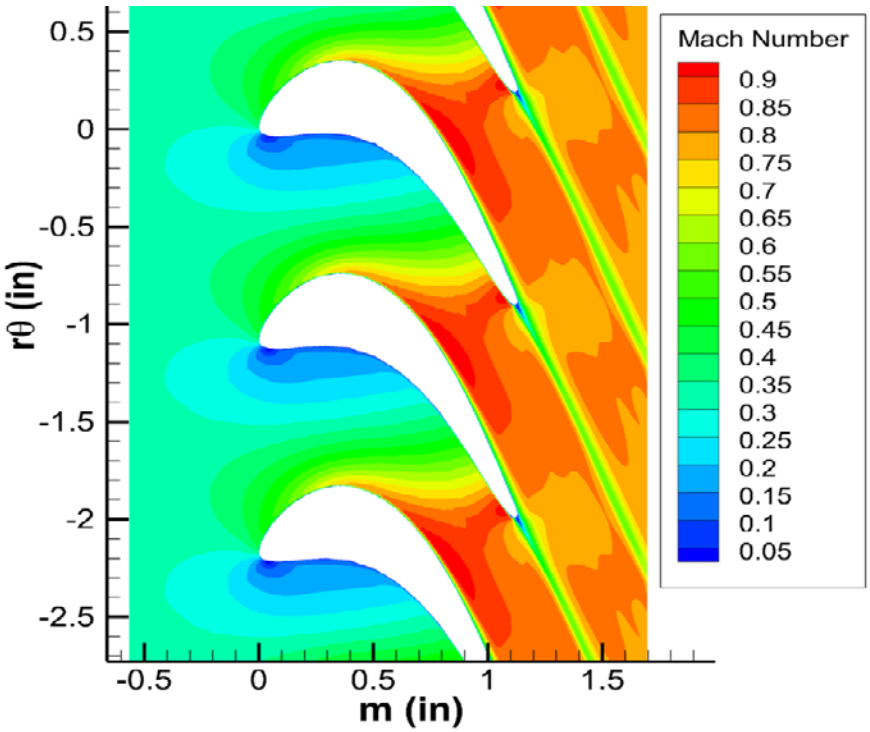

Figure 43. EEE Rotor 1 Run 2 Mach No. w/no Heat Considerations

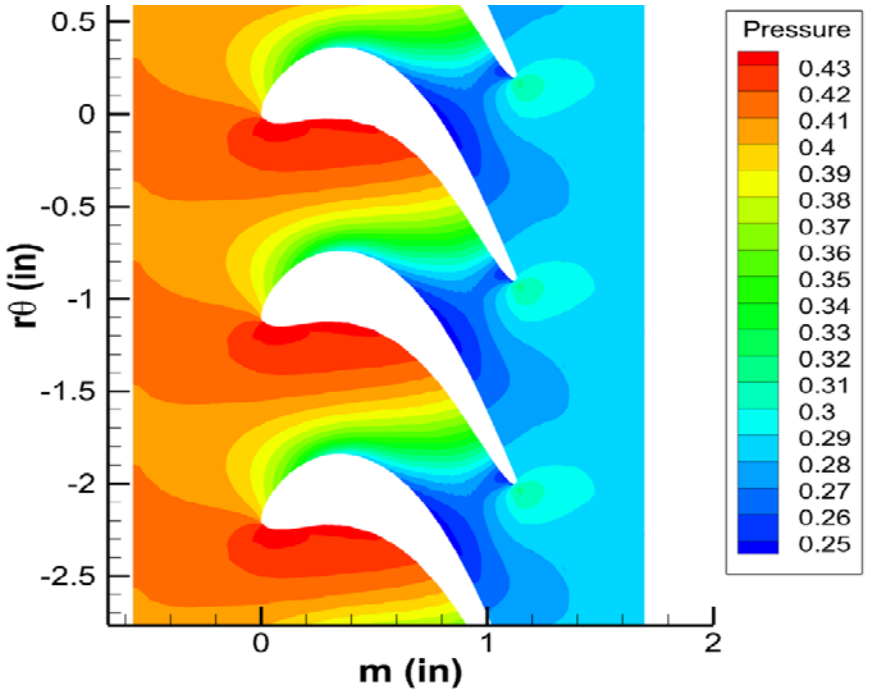

Figure 44. EEE Rotor 1 Run 3 Pressure w/no Heat Considerations

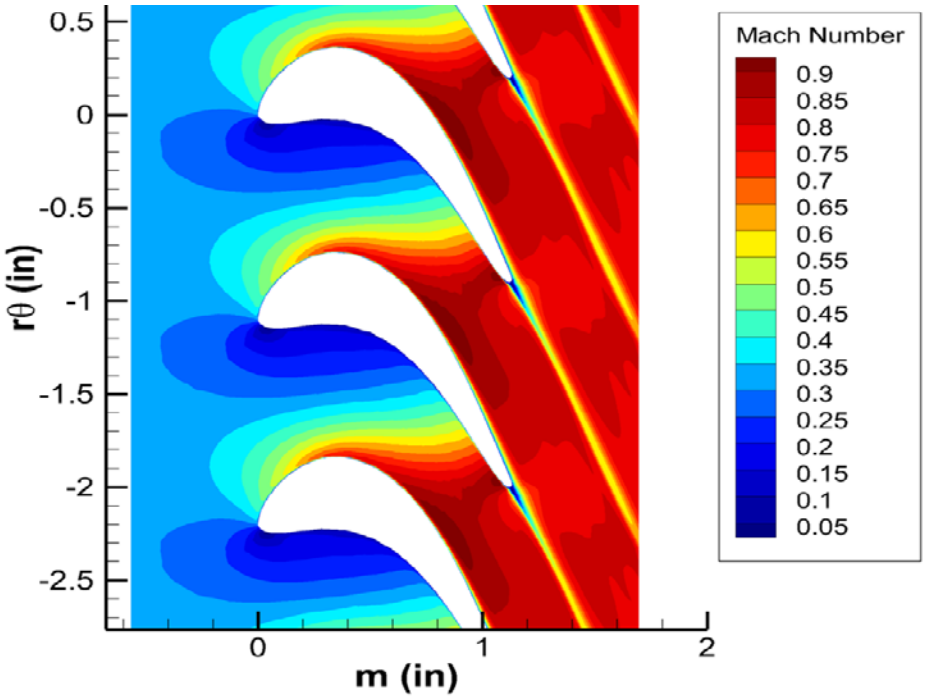

Figure 45. EEE Rotor 1 Run 3 Mach No. w/no Heat Considerations

From Table 9, we can see that optimizing for efficiency and tangential momentum have increased by almost 0.1% and 1.13%, which is of course expected because the EEE had years of experimental work to improve the efficiency. So, a huge efficiency increase is not expected and if a large increase did that would show that the blade from the direct design was not a good design. Overall, the fitness value increased by 1.2% for the best run, which was Run 1.

Table 9. EEE Rotor 1 Fitness Values w/no Heat Considerations

Case	OBJ_Final	OBJ(1)	OBJ(2)
Initial	85.480	92.44	85.480
Run 1	86.528	92.5216	86.452
Run 2	86.297	92.553	86.192
Run 3	86.380	92.5531	86.275

From Figure 46, we can see that the optimized blades have converged and all show that the pressure side curvature increasing to increase the pressure force exerted on the blade. The curvature also increases on the suction side, which helps improve blade flow as well. The blade area does not really decrease, which is due to the surface area condition being met to ensure that the blade does not get too small for structural considerations. Again, the TE keeps the same curvature because it is constrained in the mutation scheme derived earlier. Because of the blade convergence, we can deduce that there was not much to improve for the rotor section; however, the efficiency increase is well worth it for only spending a third of a day running the simulation.

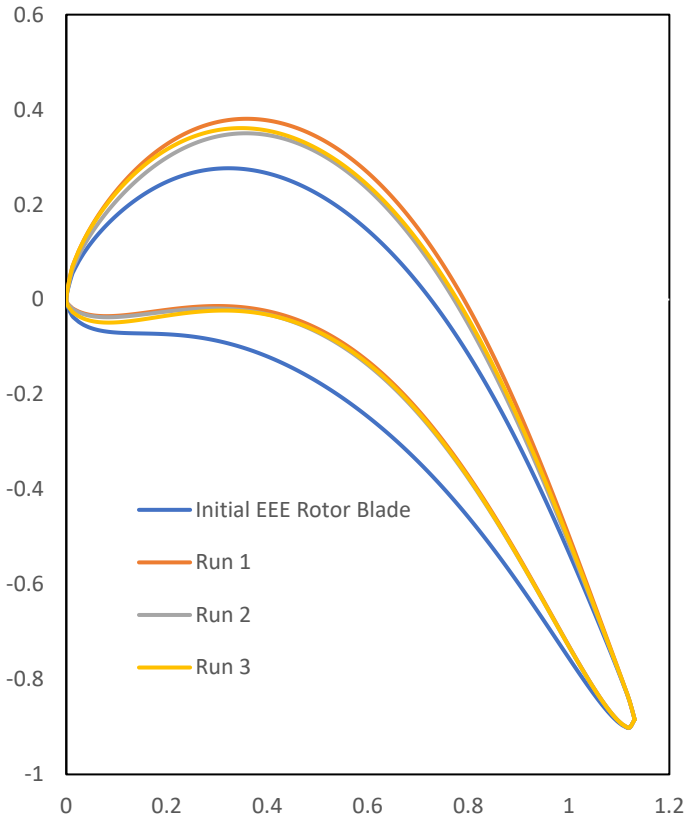

Figure 46. Comparison of Final Rotor Geometries w/no Heat Considerations

Now with thermal parameters considered the blade shape changes even more. Looking at Figure 47, a considerable curvature increase is noticed on the suction and pressure side. This blunt shaped curvature was also noticed from Curriston [2] & Thorn [3], so this result was expected. Also, compared to the rotor blades with no thermal considerations, we can see an increased bubble of high pressure elongating down the blade, because we are optimizing for power output, there is an increased amount of pressure being exerted on the blade. Again, we see this effect, which is shown on Figure 48, through the Mach number contours and we see the increased bubble region of lower velocity that is resulting in a higher-pressure region.

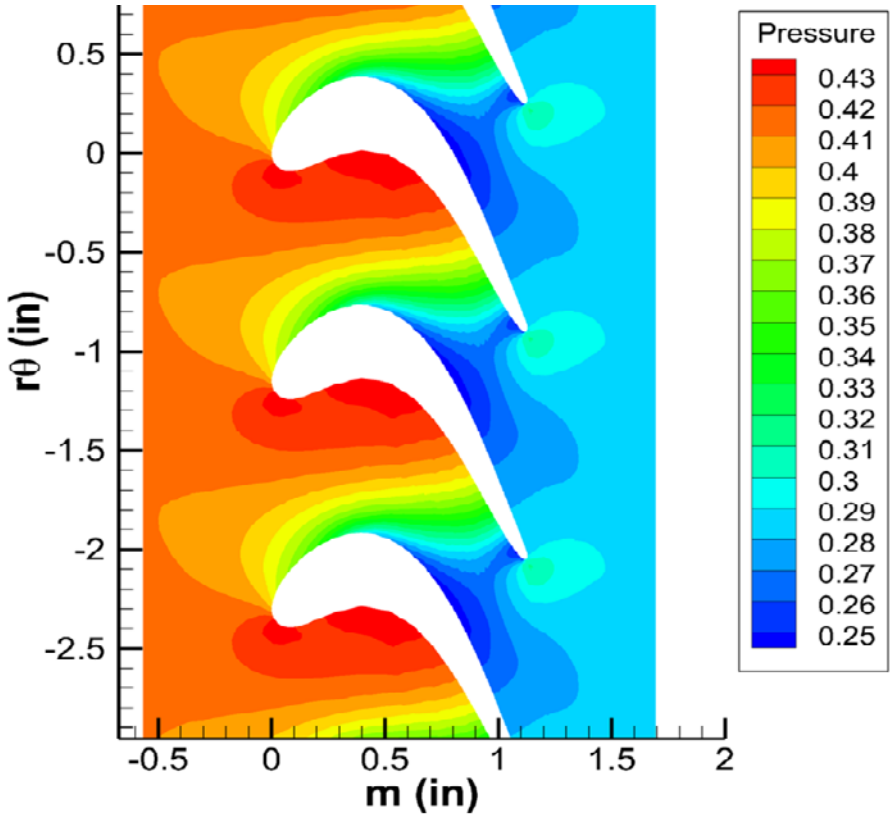

Figure 47. EEE Rotor 1 Run 1 Pressure with Heat Considerations

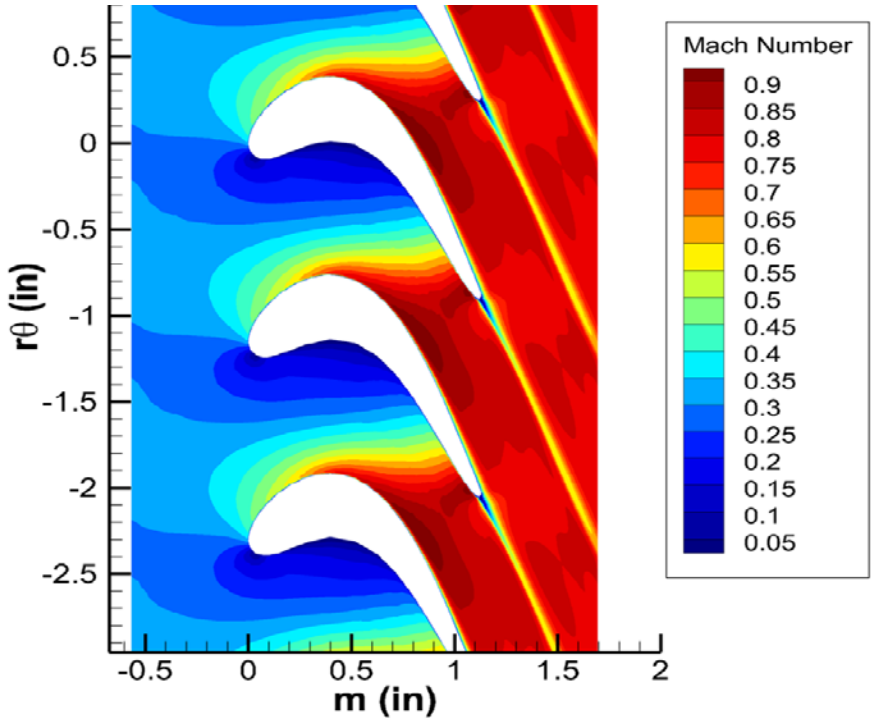

Figure 48. EEE Rotor 1 Run 1 Mach No. with Heat Considerations

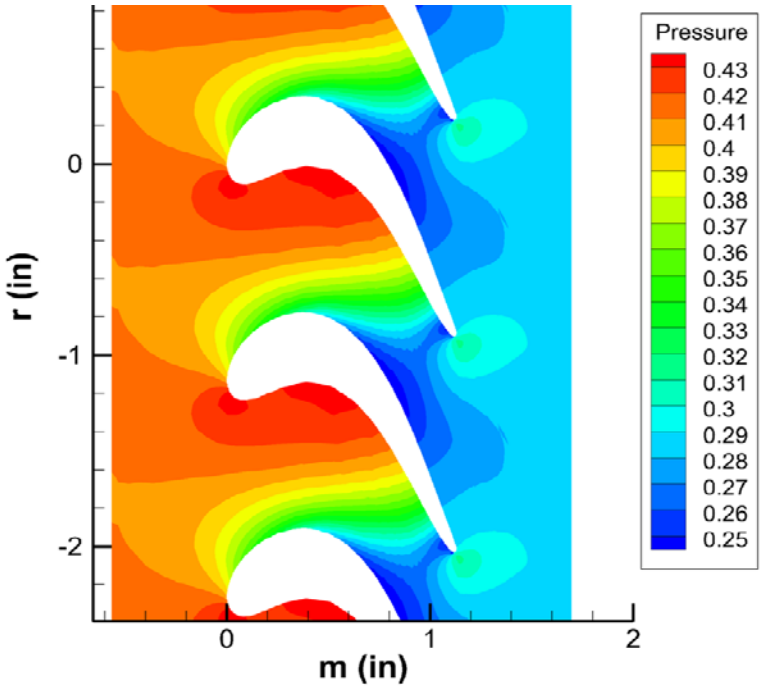

Figure 49. EEE Rotor 1 Run 2 Pressure with Heat Considerations

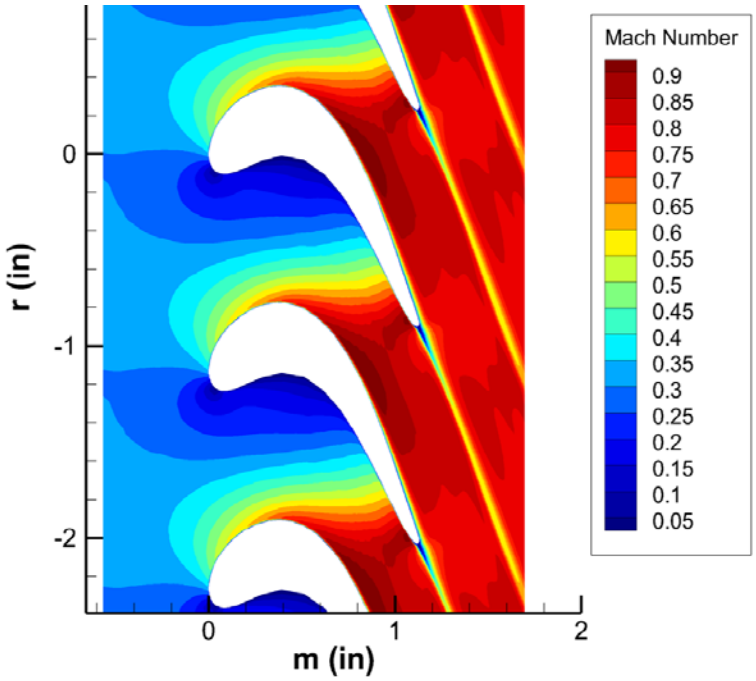

Figure 50. EEE Rotor 1 Run 2 Mach No. with Heat Considerations

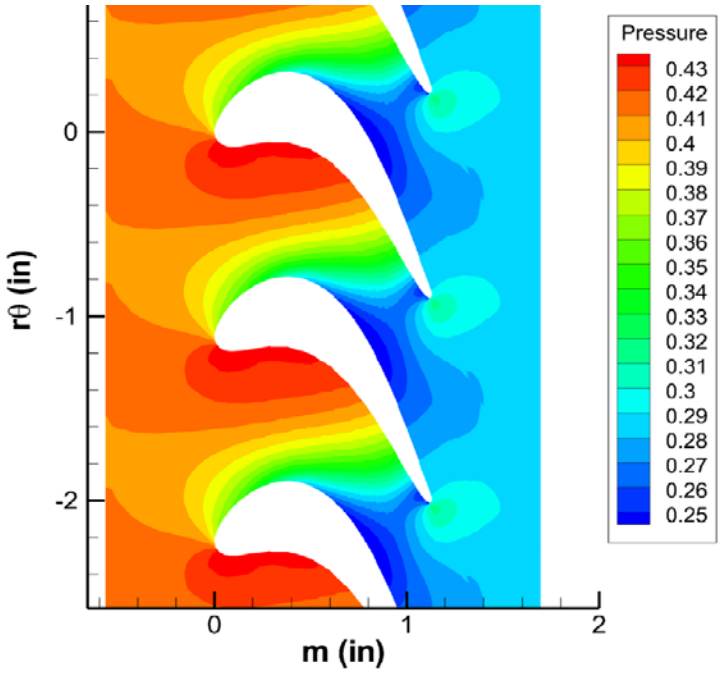

Figure 51. EEE Rotor 1 Run 3 Pressure with Heat Considerations

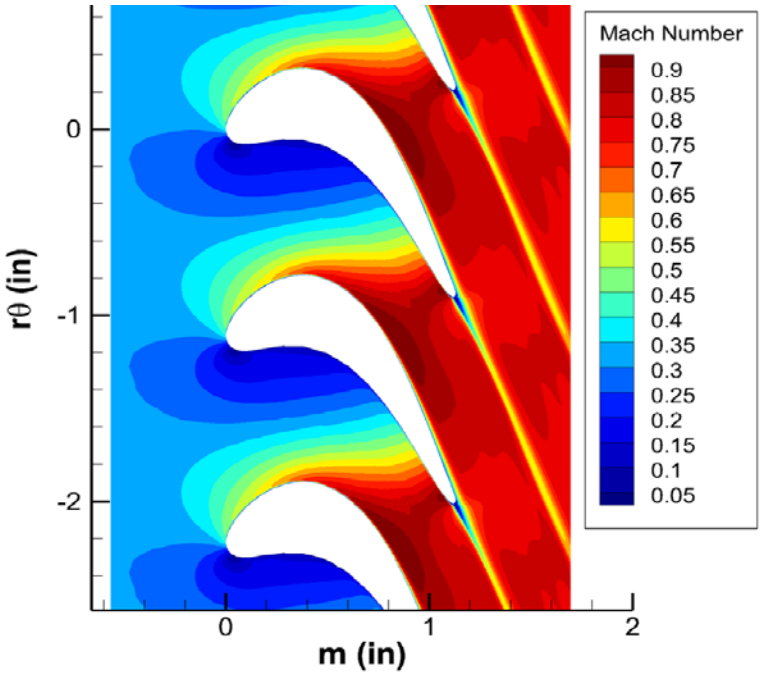

Figure 52. EEE Rotor 1 Run 3 Mach No. with Heat Considerations

For this case the overall fitness was capable of being increased further than the runs with no thermal considerations. However, for these runs the efficiency barely increases, while the work increases, and there was more room to increase the shaft power. For run 1, the best run, the efficiency was increased by 0.07%, tangential momentum increased by 1.26%, power increased by 3.95%, the max allowable temperature increased by 5.9%, and an overall fitness increase of 5.27%. An important feature to notice, is that even though one parameter increases it does not guarantee a one-to-one increase, nor does it guarantee that the other parameters will even increase at all. Also, from Figure 53, clearly the blades are converging to the run 1 blade and the downward curvature on the pressure side that was not seen from Figure 46 became a more blunt shaped blade. Because the optimizer includes the tangential momentum term we can see the upward curvature form to generate a high-pressure region on the LE region as well.

Table 10. EEE Rotor 1 Fitness Values with Heat Considerations

	Obj_Final	Obj(1)	Obj(2)	Obj(3)	$T_{0.new}/T_{0,old}$
Initial	85.4808	92.44	85.48	1	1
Run 1	89.990072	92.446461	86.562	1.0394572	1.0597112
Run 2	89.629537	92.448587	86.401	1.0371742	1.0562564
Run 3	88.948779	92.441653	86.26	1.0311338	1.0471153

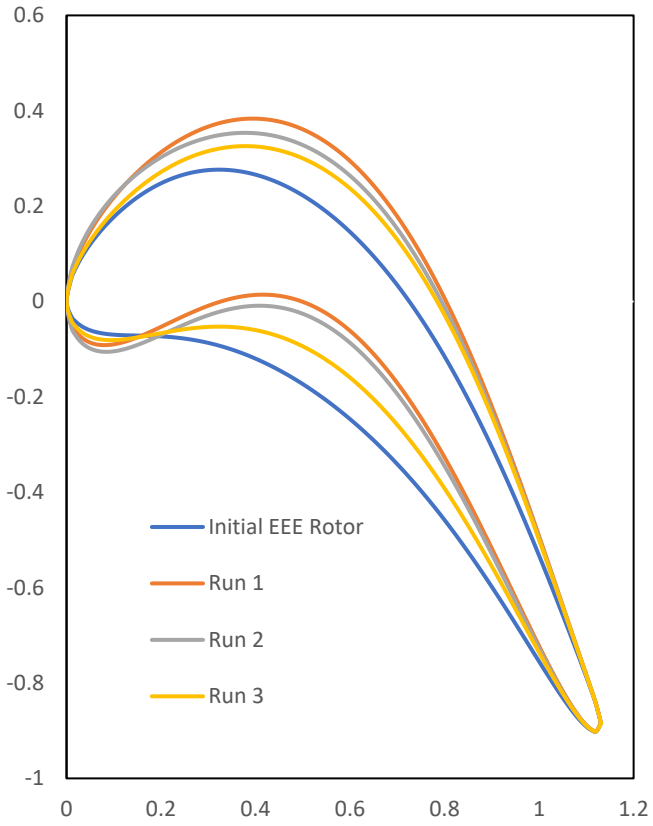

Figure 53. Comparison of Final Rotor 1 Geometries with Heat Considerations

5.3 NASA Rotor 37

For the turbine, we seen that there were more constraints that could be moved around to change the blade shape and still achieve a feasible flow. However, the turbine experiences a favorable pressure gradient, thus it does not experience the same turbulence as the compressor. The compressor induces an adverse pressure gradient to increase the low pressure to a high pressure, therefore the parameters we sought to minimize in the turbine are by nature inherit to the compressor, so penalizing the adverse pressure gradient is not useful in this section. Because of the adverse pressure gradient contributing to flow separation, we would expect that there is a very limited percent change the blade can experience. However, we do see that there is huge change in the exit pressure. Also the exit pressure has increased its region of influence, shown on Figure 54, and is a layer that is constant in the $r\theta$ direction compared to Figure 23, which only has bubbles of high exit pressure. Through the Mach number contours on Figure 55, show the effects of blade shape are different as well because the region above the suction LE has a much higher velocity compared to Rotor 37, and a more uniform velocity in the throat section contributing to a higher exit pressure.

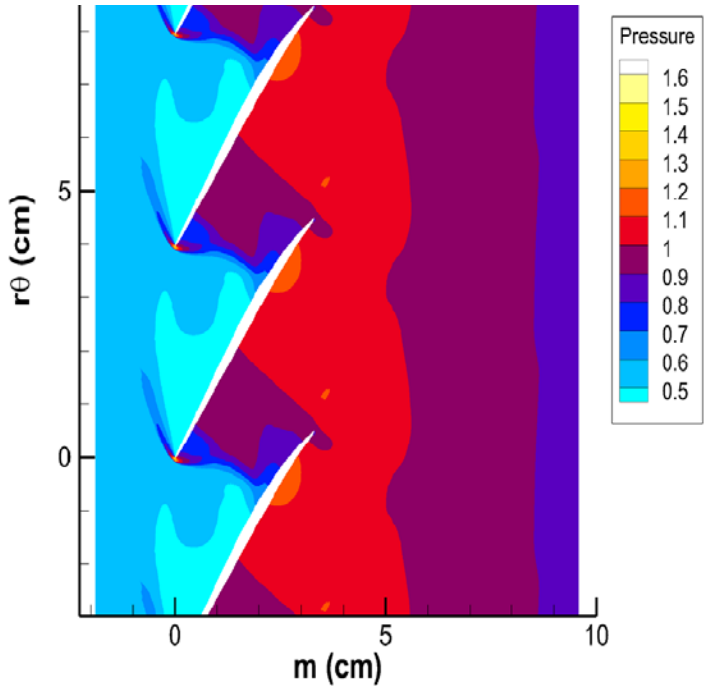

Figure 54. Rotor 37 Run 1 Pressure

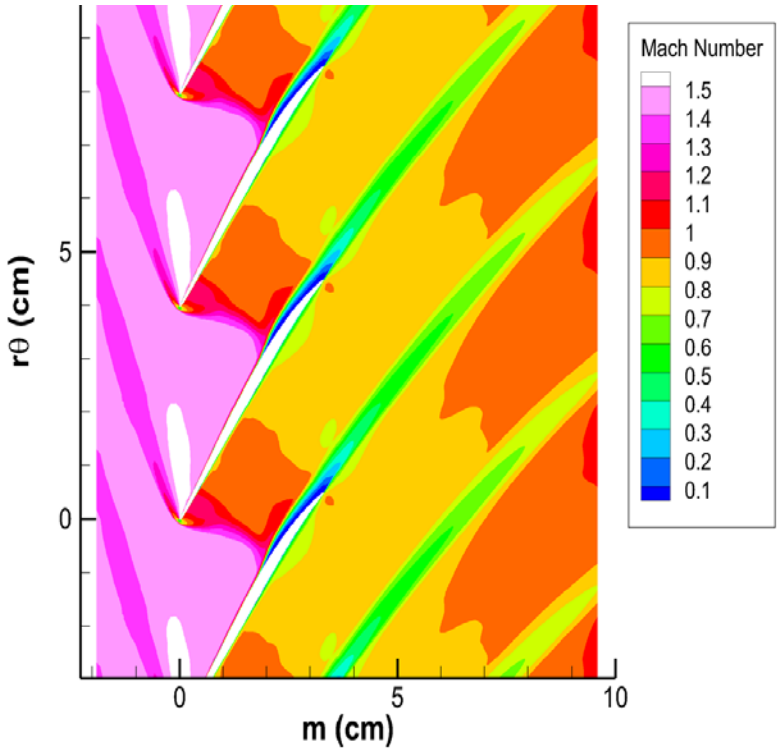

Figure 55. Rotor 37 Run 1 Mach Number

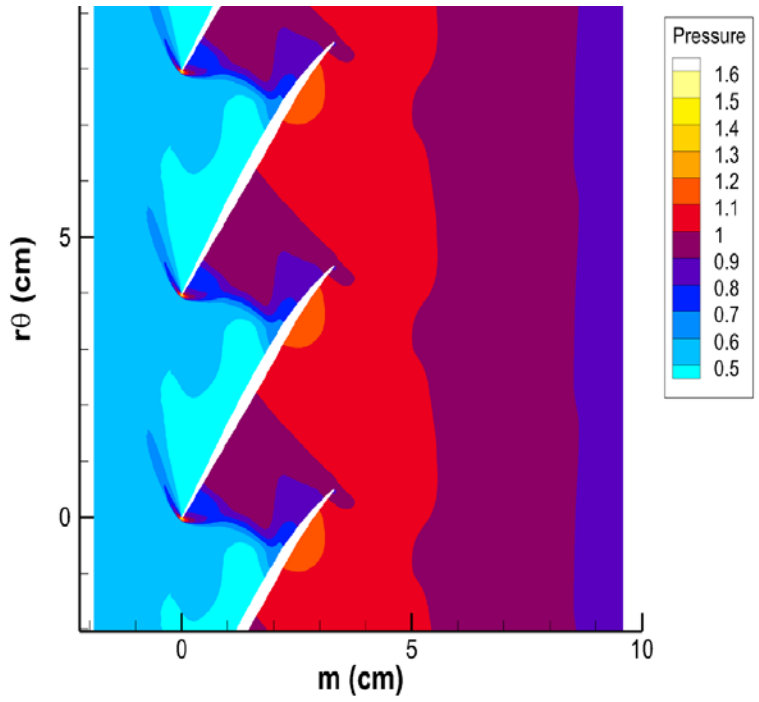

Figure 56. Rotor 37 Run 2 Pressure

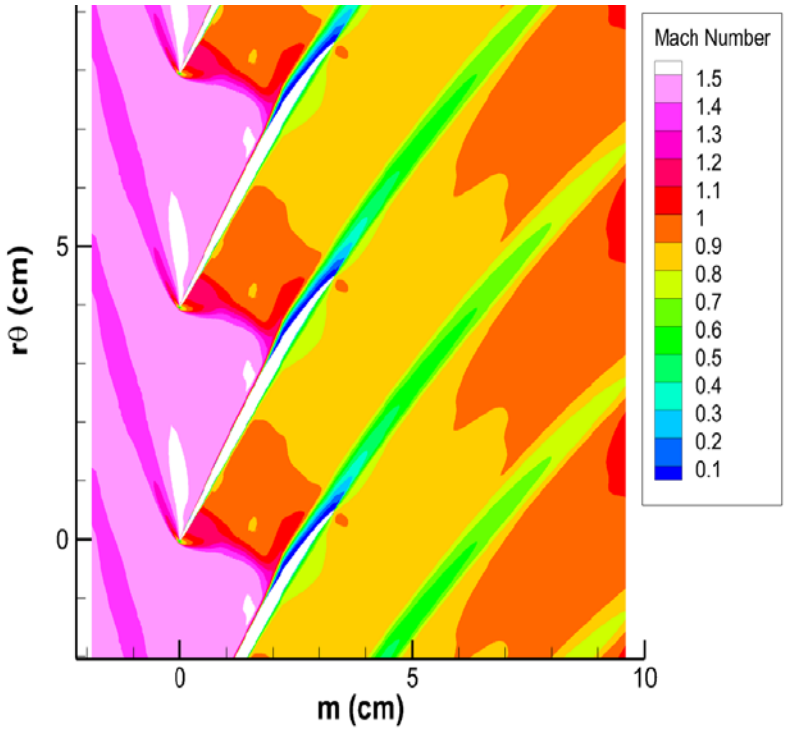

Figure 57. Rotor 37 Run 2 Mach Number

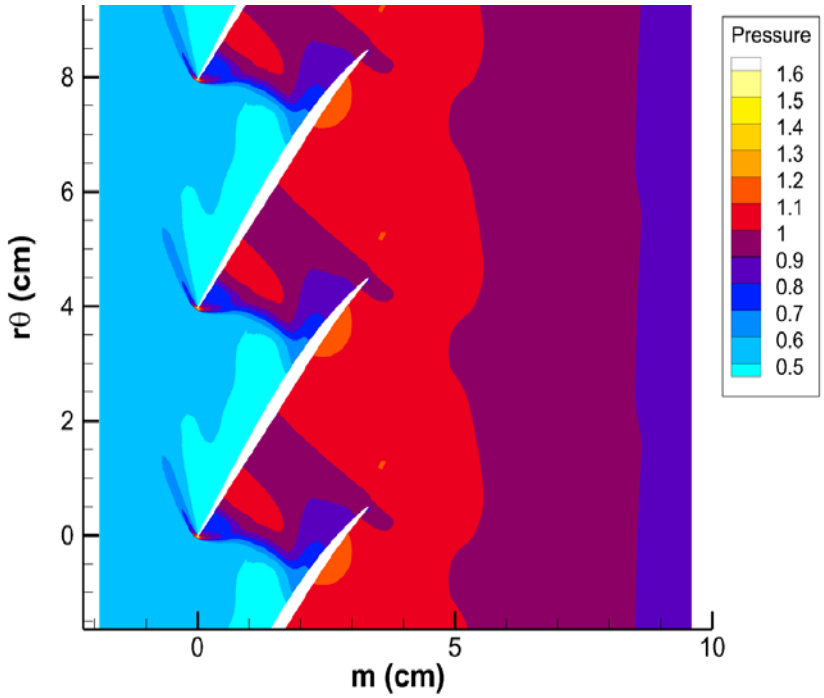

Figure 58. Rotor 37 Run 3 Pressure

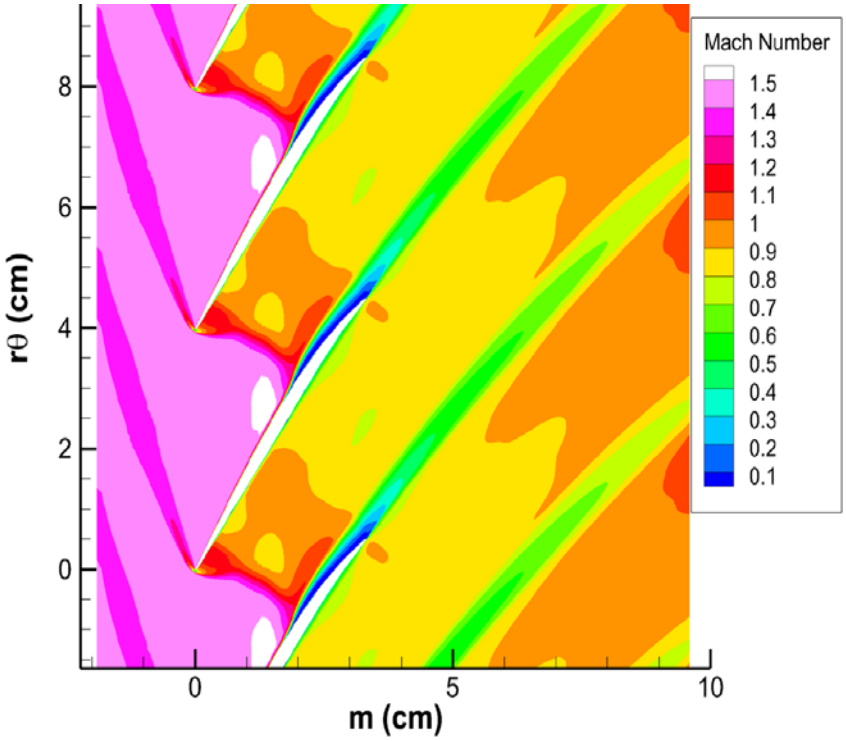

Figure 59. Rotor 37 Run 3 Mach Number

From Table 11, the efficiency increases by 2.52%, pressure ratio increases by 2.5%, and the overall fitness increases by 5.08%. These numbers are very similar to those of [31], however, their blade configuration had different conditions and did not utilize the CST methodology. The numbers presented here show a slight increase compared to [31], because their blade was a three-dimensional blade and it is expected that the overall pressure ratio would be less if the blade included the hub and tip sections. However, this analysis is very useful in that it was able to be verified from published results and that the CST methodology can produce a blade which has realistic features. So, looking at the final blade we can see the blade only changes significantly on the suction mid chord region for all three cases. Also, the blades converged on top of each other and are displayed separately to visualize the optimized change.

Table 11. Rotor 37 Fitness Values

Case	OBJ_Final	OBJ(1)	OBJ(2)
Rotor 37	1.8417	2.0977	0.87797
Run 1	1.9352691	2.1503575	0.8999755
Run 2	1.9353569	2.150236	0.9000672
Run 3	1.9192516	2.1458844	0.8943872

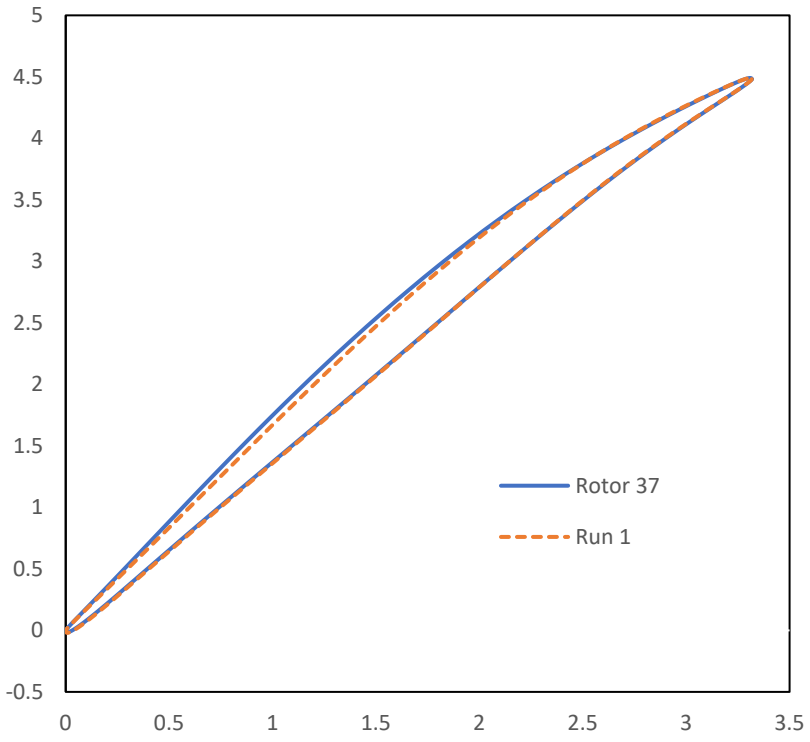

Figure 60. Rotor 37 Run 1 Optimized Blade

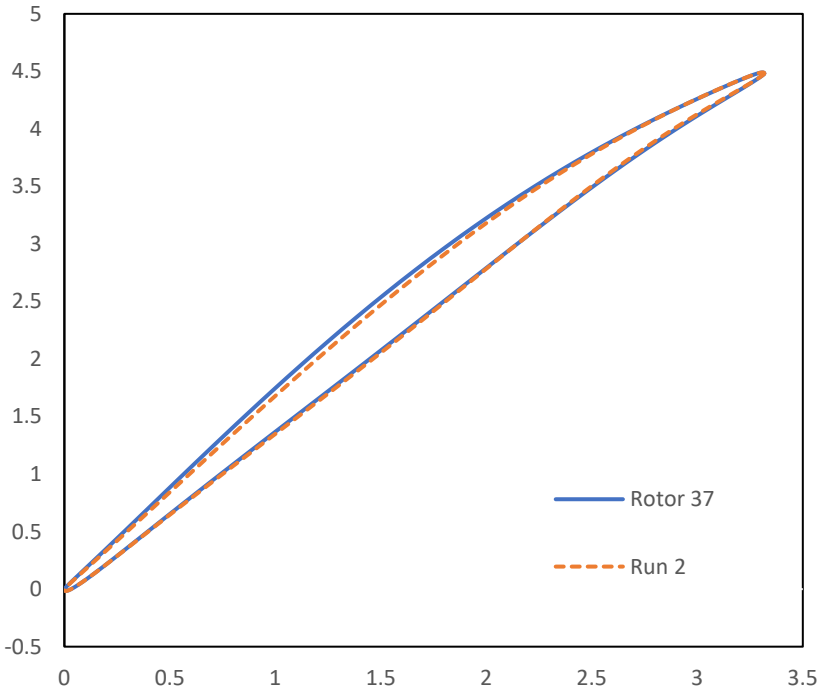

Figure 61. Rotor 37 Run 2 Optimized Blade

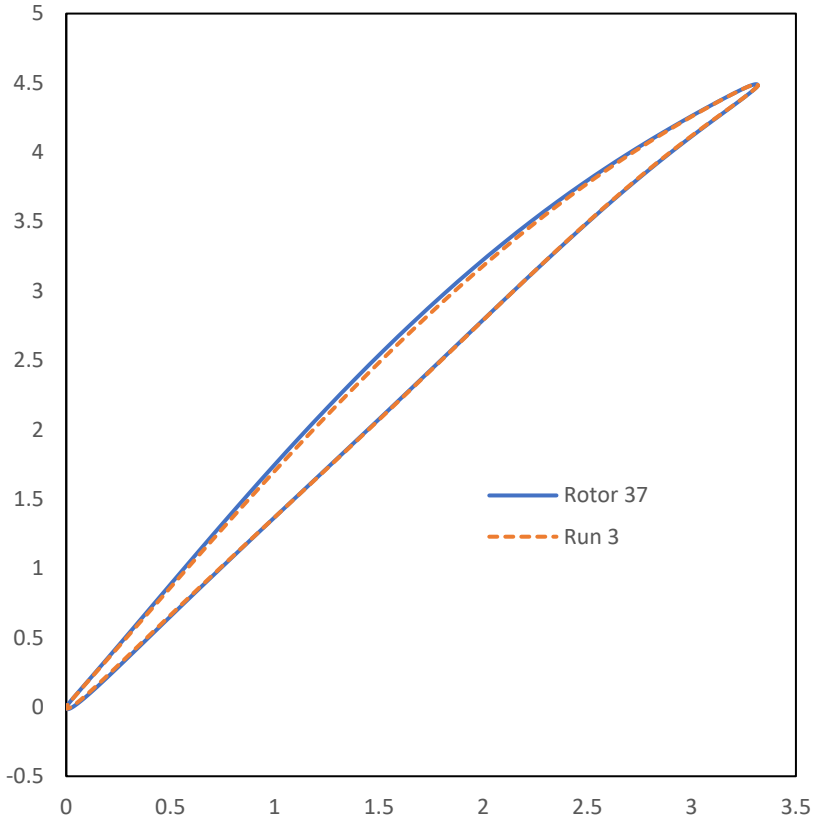

Figure 62. Rotor 37 Run 3 Optimized Blade

Chapter 6

Conclusions

From the results, clearly the CST methodology is useful for producing physical blades which have the characteristics of an actual leading and trailing edge. The compressor results were able to be verified against previous studies who utilized Bezier curves. Therefore, it important to realize that the CST methodology could be an important design tool for airfoil type configurations such as turbomachinery and could be useful for more optimizations studies. Future studies will have to include the three-dimensional CST methodology and compare it to the hybrid NURBs function from Thorn [3]. The turbine results showed promising results and the blades configured themselves into shapes which had similar features to those of Curriston [2]. Again, it is important to see that CST method was able to produce the blunt shaped leading that was expected for the turbine case with thermal considerations.

From this study we know that there are several major design factors not included such as lean, sweep, and twist which have been shown to change in the optimization scheme, therefore a three-dimensional study needs to be done to show the full effects of tip clearance, rotor/stator interactions, secondary flow, etc. However, this study was to only verify the CST methodology was capable of modeling two-dimensional blades and that the ES method could mutate the blades and show improved performance.

For future work, the three-dimensional case will be applied to the turbine and compressor, but more importantly the multistage CFD solver SWIFT and TCGRID will be utilized to optimize blades simultaneously, rather than sequentially. Once again, this study was able to prove that the Evolutionary Strategies is a very powerful optimizer allowing for a quick and simple optimization

without requiring neural network solvers. Also, this study shows that there is room for improvements on compressors and the next major goal will be to simultaneously optimize a full compressor stage with stators and rotors. Future studies will also implement neural networks to speed up the optimization process for learning the optimal search space quicker than ES can provide. Parallel processing is also a new feature that needs to be implemented to drastically decrease computation time for optimization studies since there are many CFD evaluations that need to be completed.

References

[1] *Spot Prices for Crude Oil and Petroleum Products*, U.S. Energy Information Administration, www.eia.gov/dnav/pet/PET_PRI_SPT_S1_M.htm

[2] Curriston, D. A., "Turbine Aerothermal Optimization Using Evolution Strategies," Master's Thesis, Aerospace Engineering, Auburn University, Auburn, AL, 2014

[3] Thorne, C. R., "Optimization of a Turboramjet hot section with an Interstage Turbine Burner," Ph. D. Dissertation, Aerospace Engineering, Auburn University, Auburn, AL, 2016

[4] Chima, R. V., "GRAPE 2-D Grid Generator for Turbomachinery User's Manual and Documentation Version 107," May 2011

[5] Steger, J. L., Sorenson, R. L., "Automatic Mesh Point Clustering Near a Boundary in Grid Generation with Elliptic Partial Differential Equations," Journal of Computational Physics, Vol. 33, No. 3, Dec. 1979, pp. 405-410

[6] Sorenson, R. L., "A Computer Program to Generate Two-Dimensional Grids About Airfoils and Other Shapes by Use of Poisson's Equation," NASA TM-81198. 1980

[7] Chima, R. V., "RVCQ3D Rotor Viscous Code Quasi-3-D User's Manual and Documentation Version 406," May 2011

[8] Curriston, D. A., Hartfield, R. J., "Power Turbine Blade Aerodynamic Optimization Using Non-Restrictive Evolution Strategies," 49th AIAA/ASME/SAE/ASEE Joint Propulsion Conference, AIAA Propulsion and Energy Forum, (AIAA 2013-3685)

[9] Curriston, D. A., Hartfield, R. J., "Turbine Blade Aerothermal Optimization Using Evolution Strategies," 50th AIAA/ASME/SAE/ASEE Joint Propulsion Conference, AIAA Propulsion and Energy Forum, (AIAA 2014-3521)

[10] Thorn, C. R., Hartfield, R. J., "Multi-row Turbine Blade Aerothermal Optimization Using Evolution Strategies with Viscous Flow Analysis," 51st AIAA/ASME/SAE/ASEE Joint Propulsion Conference, AIAA Propulsion and Energy Forum, (AIAA 2015-4130)

[11] Thorn, C. R., Hartfield, R. J., "Three-Dimensional Turbine Blade Optimization Using Evolutionary Algorithm with Viscous Flow Analysis," 54th AIAA Aerospace Sciences Meeting, AIAA SciTech Forum, (AIAA 2016-0115)

[12] Chima, R. V., "Analysis of Inviscid and Viscous Flows in Cascades with an Explicit Multiple-grid Algorithm," AIAA JOURNAL, Vol. 23, No. 10, pp. 1556-1563

[13] Chima, R. V., "A κ-ω Turbulence Model for Quasi-three-dimensional Turbomachinery Flows," AIAA 34th Aerospace Sciences Meeting and Exhibit, Reno, (AIAA 1996-0248)

[14] Chima, R. V., Giel, P. W., Boyle, R. J., "An Algebraic Turbulence Model for Three-Dimensional Viscous Flows," 31st Aerospace Sciences Meeting and Exhibit, (AIAA 1993-0083)

[15] Chima, R. V., "Application of the κ-ω Turbulence Model to Quasi-Three-Dimensional Turbomachinery Flows," Journal of Propulsion and Power, Vol. 12, No. 6, pp. 1176-1179

[16] Chima, R. V., "Calculation of Multistage Turbomachinery Using Steady Characteristic Boundary Conditions," 36th AIAA Aerospace Sciences Meeting and Exhibit, Aerospace Sciences Meetings, (AIAA 1998-0968)

[17] Baskharone, E. A., *Principles of Turbomachinery in Air-Breathing Engines*, Cambridge University Press, New York, 2006

[18] Flack, R. D., *Fundamentals of Jet Propulsion with Applications,* Cambridge University Press, New York, 2005
[19] Cumpsty, N. A., *Compressor Aerodynamics,* Krieger Publishing Company, Florida, 2004
[20] Wilson, D. G., Korakianitis, T., *The Design of High-Efficiency Turbomachinery and Gas Turbines,* The MIT Press, Massachusetts, 2nd Ed., 2014
[21] Aungier, R. H., *Turbine Aerodynamics,* ASME, New York, 2006
[22] Aungier, R. H., *Axial-Flow Compressors,* ASME, New York, 2003
[23] Hill, P., Peterson, C., *Mechanics and Thermodynamics of Propulsion,* Pearson, 2nd Ed., 1991
[24] Dreo, J., Petrowski, A., Siarry, P., Taillard, E., *Metaheuristics for Hard Optimization Methods and Case Studies,* Springer-Verlag Berlin Heidelberg, New York, 2006
[25] Farin, G., Hansford, D., *The Essentials of CAGD,* A K Peters, Massachusetts, 2000
[26] Kulfan, B. M., Bussoletti, J. E., ""Fundamentals" Parametric Geometry Representations for Aircraft Component Shapes," 11th AIAA/ISSMP Multidisciplinary Analysis and Optimization Conference, (AIAA 2006-6948)
[27] Burger, C., Hartfield, R. J., Burkhalter, J. E., "Performance and Noise Optimization of a Propeller using the Vortex Lattice Method and a Genetic Algorithm," 3rd AIAA Multidisciplinary Design Optimization Specialist Conference, (AIAA 2007-1883)
[28] Samad, A., Kim, K. Y., "Shape Optimization of an Axial Compressor Blade by Multiobjective Genetic Algorithm," Proceedings of the Institution of Mechanical Engineers, Part A: Journal of Power and Energy, Vol. 222, Issue 6, pp. 599-611
[29] Lane, K. A., Marshall, D. D., "A Surface Parameterization for Airfoil Optimization and High Lift 2D Geometries Utilizing the CST Methodology," 47th AIAA Aerospace Sciences Meeting Including the New Horizons Forum and Aerospace Exposition, (AIAA 2009-1461)
[30] Timko, L. P., "ENERGY EFFICIENT ENGINE High Pressure Turbine Component Test Performance Report," NASA CR-168289
[31] Samad, A., Kim, K. Y., Goel, T., Haftka, R. T., Shyy, W., "Multiple Surrogate Modeling for Axial Compressor Blade Shape Optimization," Journal of Propulsion and Power, Vol. 24, No. 2, pp 301-310

Appendix A

Evolutionary Strategies Skeleton Code

```
Randomly select initial population of size μ
Until stopping criteria is met {
    For I = 1 to μ {
        Select parent from μ with uniform probability
        Mutate to form λ/μ children
        I++}
    μ best solutions from μ + λ replace population
}
```

Appendix B

NASA Rotor 37 GRAPE Input File

```
&grid1 jmax=311 kmax=63 ntetyp=3 nairf=5 nibdst=7 nobshp=7
       jairf=137 jtebot=57 jtetop=227 norda=0 3 maxita=0 200 nout=4
       xle=.403494 xte= 3.72082 xleft=-1.5 xright=10. rcorn=0. dsi=2.e-4
&end

&grid2 nobcas=0 nle=25 nte=10 dsra=.49834 dsle=.00035 dste=.00075
       pitch= 3.99455 yscl=1. xtfrac=1. dsobi=.04
       aaai=0.45 bbbi=0.45 ccci=0.15 dddi=0.15 csmoo=0.0 jcap=33
       dswex=.4 jwakex=1 kwakex=1 joble=9 exl=1.5 exr=1.5
&end

&grid3 airfx=

       airfy=

&end
```

Appendix C

NASA Rotor 37 RVCQ3D Input File

```
&nl1 m=311 n=63 mtl=57 mil=140
&end

&nl2 nstg=4 ndis=2 ivdt=1 cfl=5.6 avisc2=.75 avisc4=1.0 irs=1 eps=1.4
        icdup=2 refm=.8 ausmk=1. hcuspk=.10
&end

&nl3 ibcin=1 ibcex=1 itmax=5000 iresti=0 iresto=1 ires=-10
        icrnt=10 ixrm=0 mioe=2
&end

&nl4 amle=.577 alle=0. bete=40. prat=1.2000 p0in=1. t0in=1. g=1.4
&end

&nl5 ilt=5 jedge=30 renr=2.1892e5 prnr=.7 tw=0. vispwr=.667 cmutm=14.0 itur=2
&end

&nl6 omega=-.05288113 nblade=36 nmn=24
&end

&nl7 tintens=.03 tmuinf=.1 hrough=0. isst=1
&end
```